J Neurophysiol 123: 392–406, 2020.
First published December 4, 2019; doi:10.1152/jn.00523.2018.

RESEARCH ARTICLE | *Nervous System Pathophysiology*

GABA bouton subpopulations in the human dentate gyrus are differentially altered in mesial temporal lobe epilepsy

Ahmad Alhourani,[1]* Kenneth N. Fish,[2]* Thomas A. Wozny,[3] Vivek Sudhakar,[4] Ronald L. Hamilton,[5] and R. Mark Richardson[6,7]

[1]*Department of Neurological Surgery, University of Louisville School of Medicine, Louisville, Kentucky;* [2]*Department of Psychiatry, University of Pittsburgh School of Medicine, Pittsburgh, Pennsylvania;* [3]*Department of Neurological Surgery, University of California, San Francisco, California;* [4]*Department of Neurological Surgery, University of Pittsburgh School of Medicine, Pittsburgh, Pennsylvania;* [5]*Department of Pathology, University of Pittsburgh School of Medicine, Pittsburgh, Pennsylvania;* [6]*Department of Neurological Surgery, Massachusetts General Hospital, Boston, Massachusetts; and* [7]*Harvard Medical School, Boston, Massachusetts*

Submitted 6 August 2018; accepted in final form 19 November 2019

Alhourani A, Fish KN, Wozny TA, Sudhakar V, Hamilton RL, Richardson RM. GABA bouton subpopulations in the human dentate gyrus are differentially altered in mesial temporal lobe epilepsy. *J Neurophysiol* 123: 392–406, 2020. First published December 4, 2019; doi:10.1152/jn.00523.2018.—Medically intractable temporal lobe epilepsy is a devastating disease, for which surgical removal of the seizure onset zone is the only known cure. Multiple studies have found evidence of abnormal dentate gyrus network circuitry in human mesial temporal lobe epilepsy (MTLE). Principal neurons within the dentate gyrus gate entorhinal input into the hippocampus, providing a critical step in information processing. Crucial to that role are GABA-expressing neurons, particularly parvalbumin (PV)-expressing basket cells (PVBCs) and chandelier cells (PVChCs), which provide strong, temporally coordinated inhibitory signals. Alterations in PVBC and PVChC boutons have been described in epilepsy, but the value of these studies has been limited due to methodological hurdles associated with studying human tissue. We developed a multilabel immunofluorescence confocal microscopy and a custom segmentation algorithm to quantitatively assess PVBC and PVChC bouton densities and to infer relative synaptic protein content in the human dentate gyrus. Using en bloc specimens from MTLE subjects with and without hippocampal sclerosis, paired with nonepileptic controls, we demonstrate the utility of this approach for detecting cell-type specific synaptic alterations. Specifically, we found increased density of PVBC boutons, while PVChC boutons decreased significantly in the dentate granule cell layer of subjects with hippocampal sclerosis compared with matched controls. In contrast, bouton densities for either PV-positive cell type did not differ between epileptic subjects without sclerosis and matched controls. These results may explain conflicting findings from previous studies that have reported both preserved and decreased PV bouton densities and establish a new standard for quantitative assessment of interneuron boutons in epilepsy.

NEW & NOTEWORTHY A state-of-the-art, multilabel immunofluorescence confocal microscopy and custom segmentation algorithm technique, developed previously for studying synapses in the human prefrontal cortex, was modified to study the hippocampal dentate gyrus in specimens surgically removed from patients with temporal lobe epilepsy. The authors discovered that chandelier and basket cell boutons in the human dentate gyrus are differentially altered in mesial temporal lobe epilepsy.

basket cell; chandelier cell; dentate gyrus; epilepsy; interneuron

INTRODUCTION

More than 30% of all patients with mesial temporal lobe epilepsy (MTLE) become refractory to pharmacological intervention (Schuele and Lüders 2008). In these cases, surgical removal or ablation of the seizure onset zone is the only potential cure. Despite at least 14 new antiepileptic drugs entering the market in the last 20 yr, the rate of refractory epilepsy has not significantly decreased (Chen et al. 2018; Dumitriu et al. 2012; Faraji and Richardson 2018). This impasse is partly due to reliance on testing of novel compounds in animal models that recapitulate an epilepsy endophenotype (e.g., seizure) but not necessarily the circuit pathology. Thus there is a critical need to improve our understanding of the underlying microcircuit pathology in humans with epilepsy (Gerlach and Krajewski 2010; Löscher 2011). This need is especially pressing in light of the current clinical trend to treat MTLE first with laser interstitial thermal therapy rather than resection (Bezchlibnyk et al. 2018), which has significantly reduced the availability to the scientific community of the type of tissue used in this study, which already was rare: hippocampal specimens removed en bloc and thus relatively intact.

Granule cells, the principal neurons within the dentate gyrus, gate entorhinal input into the hippocampus. Crucial to the role of principal neurons in information processing are the inhibitory inputs from GABA-expressing (GABAergic) neurons. In epilepsy, it is hypothesized that alterations in the gating of principal neuron excitability by GABAergic neurons result in the initiation and propagation of seizures (Dudek and Sutula 2007). GABAergic neurons are composed of phenotypically and functionally distinct subpopulations (Freund and Buzsáki 1996). Findings from mostly single-labeled anatomical studies have implicated the GABAergic neuron subpopulation that

* A. Alhourani and K. N. Fish contributed equally to this work.
Address for reprint requests and other correspondence: M. Richardson, Dept. of Neurological Surgery, Massachusetts General Hospital, Boston, MA 15213 (e-mail: mark.richardson@mgh.harvard.edu).

expresses the calcium-binding protein parvalbumin (PV) in the pathophysiology of epilepsy (Andrioli et al. 2007; Arellano et al. 2004; Sloviter et al. 1991; Wittner et al. 2001). PV-expressing neurons can be subdivided based on the principal neuron perisomatic region they target: PV basket cells (PVBCs) principally target the soma and proximal dendrites, while PV chandelier cells (PVChCs) exclusively target the axon initial segment (AIS). In human prefrontal cortex, PVBCs express the 65- and 67-kDa isoforms of glutamic decarboxylase (GAD65 and GAD67, respectively). In contrast, PVChCs only express GAD67 (Glausier et al. 2014), providing another means of differentiating the two PV subtypes at the level of their boutons. The densities of both PVBC and PVChC boutons are altered in epilepsy; however, the nature and extent of these changes remain unknown. For example, classic studies in hippocampal dentate gyrus tissue resected from patients showed that rewiring of PVBCs and PVChCs occurs with spatial heterogeneity (Wittner et al. 2001). This heterogeneous effect, however, could be driven either by ectopically positioned principal neurons or by principal neuron loss, in which case one might predict that the average density of PVBC and PVChC boutons per principal neuron would be unchanged as would the ability for them to synthesize and package GABA. Alternatively, if there is an epileptogenic process that directly affects a subset of PV neurons, one might predict that bouton protein levels of GAD67 and vesicular GABA transport would be altered.

To characterize GABA boutons, including those arising from PVBCs and PVChCs, and principal neuron density throughout the dentate gyrus in epilepsy, we adapted our integrated platform of multilabel immunofluorescence confocal microscopy and custom segmentation algorithms, which has been extensively used to define circuit alterations occurring in the cortex in schizophrenia (Fish et al. 2008; Glausier et al. 2015; Lewis et al. 2011; Rocco et al. 2016a; Sweet et al. 2010).This approach is capable of identifying putative boutons (multilabeled synaptic structures) arising from different GABAergic subtypes across large spatial expanses. Additionally, this method provides a quantitative measure of relative protein levels within synaptic boutons. Importantly, previous studies in human postmortem tissue (Fish et al. 2013) using a similar approach yielded findings matching those seen using electron microscopy (DeFelipe et al. 1985). In the current study, we performed a proof-of-concept quantitative analysis of dentate gyrus GABA bouton subpopulations in epilepsy and control tissue.

MATERIALS AND METHODS

Subjects. This study was carried out in accordance with the recommendations of the University of Pittsburgh Human Research Protection Office. The protocol was approved by the University of Pittsburgh Institutional Review Board. All subjects gave written informed consent in accordance with the Declaration of Helsinki. Hippocampal specimens were obtained from five subjects who underwent en bloc hippocampectomy during anterior temporal lobectomy for the treatment of pharmacoresistant MTLE. All subjects had a unilateral mesial temporal seizure onset confirmed by comprehensive multimodal presurgical evaluation, including intracranial monitoring in two subjects. A neuropathologist (R. L. Hamilton) reviewed the clinical specimens to confirm the presence or absence of hippocampal sclerosis as indicated in the clinical pathology report in accordance with the International League Against Epilepsy International consensus classification of hippocampal sclerosis in temporal lobe epilepsy. Healthy comparison hippocampal specimens were recovered during autopsies conducted at the Allegheny County Medical Examiner's Office (Pittsburgh, PA), after consent was obtained from the next of kin. The University of Pittsburgh's Committee for the Oversight of Research and Clinical Trials Involving the Dead and Institutional Review Board for Biomedical Research approved all postmortem procedures. An independent committee of physicians confirmed the absence of any diagnoses for each subject using the results of structured interviews conducted with family members and/or review of medical records (Hashimoto et al. 2008). To reduce biological variance between groups, and to employ a design that controlled for experimental variance, each epileptic subject was matched to one unaffected comparison subject for sex and as closely as possible for age (Table 1). Each surgical specimen was collected as a coronal section ($\geq$0.5 cm) of the en bloc resection of the hippocampal body, while the postmortem tissue was blocked in the coronal orientation at 1.0- to 2.0-cm intervals. Both were immediately immersed in 4% paraformaldehyde for 24–48 h at 4°C and then washed in a series of graded sucrose solutions and cryoprotected. Tissue blocks were sectioned at 40 μm on a cryostat and stored in a 30% glycerol/30% ethylene glycol solution at −30°C until processing for immunohistochemistry. To reduce the potential confounding effects of postmortem interval, all unaffected comparison subjects had a postmortem interval (PMI) $<$16 h, a time point previously shown to have no effect on the proteins studied here (Glausier et al. 2014; Rocco et al. 2016a).

Immunohistochemistry. For each subject, two sections containing the dentate gyrus spaced ~500 μm apart were analyzed by fluorescent confocal microscopy. Adjacent sections processed with Nissl staining were used to identify sections containing the dentate gyrus that were comparable in location along the cranio-caudal axis of the hippocampus across subjects based on the gross morphology of the dentate gyrus in the section. Two experimental runs were performed in which one section per subject was processed simultaneously and under identical conditions with all other specimens of that run according to methods previously detailed (Rocco et al. 2016b). Briefly, the sodium citrate antigen retrieval method was performed, followed by permeabilization with 0.3% Triton X-100. Sections were blocked using 20% donkey serum in PBS for 2 h at room temperature and incubated for ~72 h at 4°C in PBS containing 2% donkey serum and primary antibodies. The antibodies recognized the vesicular GABA transporter (vGAT; rabbit host; 1:500; product 131003, lots 131011/41 and 131011/42; Synaptic Systems, Inc.), PV [mouse host; 1:1,000; prod-

Table 1. *Subject demographics*

	Control						Epilepsy							
Subject	ID	Age, yr	Sex	PMI, h	Cause of death	Storage time, mo	ID	Age, yr	Sex	Storage time, mo	Histopathological diagnosis	Epilepsy duration, yr	Average no. seizures/mo.	Seizure Type
1	C1	40	W	9	Pulmonary hypertension	298	E1	37	W	20	Nonsclerotic	8	12	Focal with loss of awareness, secondarily generalizing
2	C2	50	M	4.5	Cardiac atherosclerosis	303	E2	49	M	28	Nonsclerotic	32	16	
3	C3	36	M	4.5	Motor vehicle accident	302	E3	40	M	46	Sclerotic	27	3	
4	C4	46	M	7.3	Motor vehicle accident	300	E4	43	M	41	Sclerotic	43	3	
5	C5	46	W	4.5	Trauma	308	E5	47	W	27	Sclerotic	45	4	

W, woman; M, man; PMI, post mortem interval.

uct 235, lot 10–11(F); Swant, Inc.], GAD65 (guinea pig host, 1:500, product 198104, lot 198104/5; Synaptic Systems, Inc.), and GAD67 (goat host; 1:100; product AF2086, lot KRD01; R&D Systems, Inc.). The specificity of each antibody was verified in our laboratory (Fish et al. 2011; Rocco et al. 2016b) or other laboratories [vGAT (O'Sullivan et al. 2016), GAD67 (Mayerl et al. 2014), and PV (Celio et al. 1988)]. Sections were rinsed for 2 h in PBS and incubated for 24 h in PBS containing 2% donkey serum and secondary antibodies (donkey host) conjugated to Alexa 488 (PV), 568 (GAD65), and 647 (GAD67) (1:500 for all) (Invitrogen, Inc.) and anti-rabbit immunoglobulin G conjugated to biotin (1:200, product 43R-1448, lot C13031123; Fitzgerald, Inc.) at 4°C. Finally, sections were rinsed for 2 h in PBS and incubated for 24 h in PBS containing 2% donkey serum and streptavidin 4°C (Alexa 405 for vGAT; Invitrogen, Inc.). After being washed, sections were mounted (ProLong Gold antifade reagent; Invitrogen, Inc.) on slides that were coded to conceal diagnosis and subject number and stored at 4°C until imaged.

Microscopy. Data were collected on an Olympus IX81 inverted microscope equipped with an Olympus spinning disk confocal unit, Hamamatsu EM-CCD digital camera, and high-precision BioPrecision2 XYZ motorized stage with linear XYZ encoders, using a ×60 1.40 numerical aperture super-corrected oil immersion objective. The equipment was controlled by SlideBook 6.0 (Intelligent Imaging Innovations, Inc.), which was the same software used for deconvolution. Three-dimensional image stacks (2-dimensional images successively captured at intervals separated by 0.25 μm in the *z*-dimension) that were 512 × 512 pixels (~137 × 137 μm) were acquired over 50% of the total thickness of the tissue section starting at the coverslip. Importantly, imaging the same percentage of the tissue section thickness rather than the same number of micrometers controls for the potential confound of storage and/or mounting related volume differences (i.e., *z*-axis shrinkage). The stacks were collected using optimal exposure settings (i.e., those that yielded the greatest dynamic range with no saturated pixels), with differences in exposures normalized during image processing.

Sampling. The boundaries of the dentate granule cell layer were masked in every section and used to construct a sampling grid. Twenty-five to thirty systematic randomly sampled image stacks within the sampling grid were taken for each section (Fig. 1*A*), resulting in 523 image stacks from all the sections. The imaging fields were centered on the dentate granule cell layer, such that the boutons captured were on the proximal dendrites, soma, and axon initial segment of dentate granule neurons, collectively representing the perisomatic innervation of dentate granule neurons. In epileptic samples, the boundaries for the granule cell layer accounted for granule cell dispersion, if present. Lipofuscin autofluorescence is a potential confound of quantitative fluorescence measures in human tissue. To address this issue, lipofuscin was imaged using a fifth custom channel (equivalent to excitation 405 nm/emission 647 nm) at a constant exposure time across all sections. A lipofuscin mask was created using a single optimal threshold value. Any object mask overlapping any voxel of the lipofuscin mask was excluded from further analysis. Importantly, lipofuscin fluorescence intensity did not differ between epilepsy [792 ± 52 arbitrary units (a.u.)] and comparison subjects (787 ± 72 a.u; paired *t* statistic: 0.12, *P* value: 0.9).

Cell counting. We quantified bouton density based on the number of cells in a given field rather than the volume of the field. We used the background staining seen in the raw images of the 488 nm channel to count the number of cell bodies in each section. An unbiased counting frame was used to identify the cell density in each image stack. A 308 × 308 pixel frame centered in the middle of each stack was made in ImageJ (Sidhu et al. 2006). Only cells within the counting frame and not on the exclusion borders were counted (Fig. 1*B*). To confirm the accuracy of this method, an additional experiment in adjacent sections from the three controls was performed using NeuN (guinea pig host, 1:500, product, ABN90, lot: 2299615; Millipore, Inc.) in the 568-nm channel and PV in the 488-nm channel. The average cell count using the NeuN maker (42.4 ± 9.5 cells/site) was not significantly different from the average cell count using the 488-nm channel background fluorescence (39.5 ± 8.4 cells/site) (Wilcoxon rank sum test, *z* value: 1.01; *P* value: 0.3).

Image processing. Accurate differentiation of fluorescent boutons requires addressing the point spread function (PSF) of fluorescent objects. To that end, we first deconvolved each fluorescent channel using the AutoQuant blind deconvolution algorithm (Media Cybernetics, Inc.). Next, the images were filtered using a three-dimensional Gaussian filter set at a width of 0.7 and 2.0 SD, respectively. A subtraction image was used to further reduce the PSF, enabling the identification of discrete fluorescent boutons as illustrated in Fig. 2. Image segmentation was performed using a modified version of a previously published algorithm (Fish et al. 2008) running entirely in MATLAB (R2015b). The compact nature of the dentate gyrus leads to partially overlapping neighboring objects and constrains the identification of separate boutons. This phenomenon leads to the erroneous exclusion of objects whose segmentation masks merge into one conglomerate mask at lower image threshold values, such that the combined mask volume exceeds the maximum size gate, even though the individual, unmerged objects are of an acceptable size. To address this problem, each mask was searched for unique objects, starting at the highest threshold mask, and these objects were then followed as they expanded in size with lowering of the threshold value. If an object was identified to have merged with another at a certain threshold value, the mask at the prior threshold value for this object was used and all the lower threshold masks for that object were discarded. A size range between 0.05 and 2 μm^3 was used. The Cartesian coordinates of the centroid of each object mask were used to virtually crop each image stack in the *x*-, *y*- and *z*-dimensions. For the *x*- and *y*- dimensions,

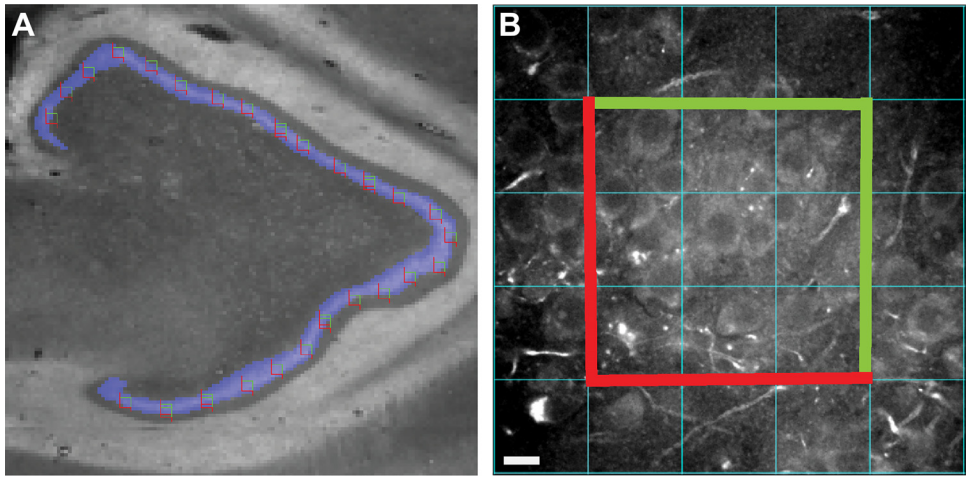

Fig. 1. Schematic of image sampling and acquisition. *A*: montage image taken at ×2 of the 568-nm channel used to create the mask (blue) of the dentate gyrus layer in a control group subject with the unbiased stereological grid sites overlaid. *B*: imaging field in a control group subject at ×60 in the 488-nm channel with the counting frame employed in cell counting shown with the exclusion borders in red and the inclusion border in green with contrast adjusted to enable accurate counting.

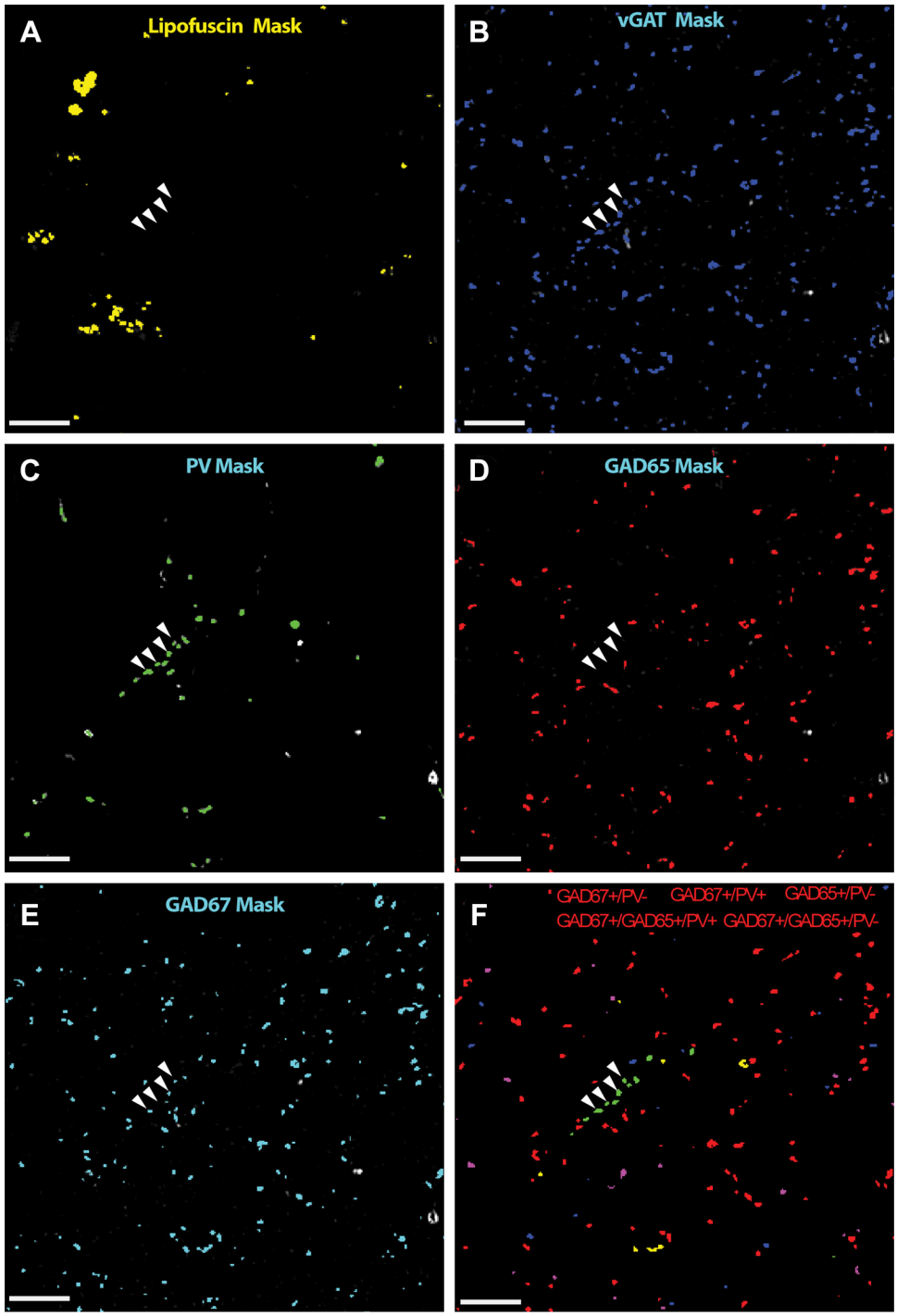

Fig. 2. Schematic of image acquisition and segmentation. *A–F*: ×2 magnified image of the counting frame from an imaging site belonging to nonsclerotic patient. The raw channel fluorescence for lipofuscin (*A*), vesicular GABA transporter (vGAT; *B*), parvalbumin (PV; *C*), glutamic decarboxylase (GAD) 65 (*D*), and GAD67 (*E*) is plotted in grayscale and the computed mask overlaid in color. *F*: composite image of the retained boutons classified based on masking operations and the naive Bayesian classifier into 5 subpopulations colored separately. Arrowheads represents a linear array of puncta classified as putative PV chandelier cell boutons based on GAD isoform protein level levels. Arrowheads are overlaid into each channel confirming that the boutons are vGAT+ (*B*), PV+ (*C*), GAD65− (*D*), and GAD67+ (*E*) and do not overlap with lipofuscin (*A*). Bar = 10 μm.

only objects with centers contained within the 308 × 308 pixels representing the counting frame were retained. For the *z*-dimension, the *z*-position of each object was normalized by the following equation:

$$Z_{\text{coordinate}} = \text{no. of } z\text{-planes invthe image stack}/40$$

Next, the objects were binned into the new 40 normalized *z*-bins. The mean object mask number and fluorescence intensity for vGAT were calculated in each *z*-bin in every image stack. An ANOVA with post hoc comparison via Tukey's test was used to identify adjacent *z*-bins that were significantly different for both measures. For both experimental runs, we selected the bins between 5 and 35 *z*-planes. Only the objects with centroids within these limits were used.

Axon bouton classification. vGAT, a protein that concentrates in GABAergic boutons and is required to package GABA for vesicular release (Chaudhry et al. 1998), is an ideal GABA bouton marker. Thus all vGAT-immunoreactive puncta were considered to be GABA boutons. The vGAT+ boutons were classified into five categories: vGAT+/GAD65+/GAD67−/PV−, vGAT+/GAD65−/GAD67+/PV−, vGAT+/GAD65+/GAD67+/PV−, vGAT+/GAD65−/GAD67+/PV+, and vGAT+/GAD65+/GAD67+/PV+. Importantly, by using a stringent definition of a GABA bouton that requires the bouton to contain both vGAT and GAD (GAD65 and or GAD67) protein, we minimized the inclusion of false positives in analyses. We adopted a two-step algorithm using masking operations for bouton classification

as described (Rocco et al. 2016b). Briefly, a set of stringent criteria for mask overlap was applied to all vGAT boutons such that a vGAT mask was considered positive for a secondary channel if two conditions were met: the centroid of the secondary mask fell inside the vGAT mask and reciprocally the centroid of the vGAT mask fell inside the secondary mask. Additionally, for a vGAT mask to be considered negative for a secondary channel, the vGAT mask had to show zero overlap with any pixels from a mask in that secondary channel. vGAT staining and masks, and their overlap with GAD, are represented in an example imaging site (Fig. 2). To increase our sensitivity for bouton detection, we applied a second step, a modified algorithm from a previously published method (Rocco et al. 2016b). Briefly, a naive Bayesian classifier was used to segregate boutons based on protein colabeling. The median GAD65 and GAD67 fluorescence intensities for the subpopulations classified using mask operations described above, which represent near perfect overlap, were used as training data for the naive Bayesian classifier. This classifier was used to segregate the remaining objects into the above categories. The PV+ and PV− objects were classified separately. Importantly, to control for the effect of total cell number between groups, bouton-density results were normalized by within-field neuron number, unless otherwise stated.

In situ hybridization. In situ hybridization probes were designed by Advanced Cell Diagnostics, Inc. (Hayward, CA) to detect mRNAs encoding GAD65 (*GAD2* gene), GAD67 (*GAD1* gene), PV (*PVALB* gene), or parathyroid hormone like hormone (*PTHLH* gene). Tissue samples were processed using the RNAscope 2.0 Assay according to the manufacturer's protocol. Briefly, tissue sections (20 μm) from the fresh-frozen right hippocampus of control subjects were fixed for 15 min in ice-cold 4% paraformaldehyde and incubated in a protease treatment, and then, the probes were hybridized to their target mRNAs for 2 h at 40°C. The sections were exposed to a series of incubations that amplified the target probes and then counterstained with DAPI.

Statistics. Data were averaged across all imaging sites in both sections for each subject; thus only one value was used per subject during statistical testing. Data are reported as means ± SD. An unpaired analysis of covariance (ANCOVA) model was used to compare group differences. Although subjects were selected and processed as pairs, a paired ANCOVA model could not be performed due to the low total subject number. Bouton density and fluorescence intensity (relative protein) level were modeled separately as the dependent variable and diagnostic group included as the main effect with age, sex, PMI, and storage time used as covariates. All statistical tests were conducted with an α-level = 0.05 and corrected for multiple comparisons using a Bonferroni correction. All reported ANCOVA *P* values are after correction. Reported ANCOVA statistics include only those covariates that were statistically significant. As a result, the reported degrees of freedom vary across analyses. Specifically, preliminary ANCOVA testing including all covariates revealed a significant relationship between *1*) storage time and fluorescence intensity of GAD65 in PV+/GAD65+/GAD67+ boutons and *2*) PV+/GAD67+ density and PMI. Those factors were included in the subsequent group comparisons to account for the covariation. Post hoc analysis was done using Tukey's honest significant difference procedure as implemented in MATLAB. Only significant mean difference values between group pairs and associated *P* values are reported.

RESULTS

Concordance with clinical diagnostic classification. Hippocampal sclerosis typically is associated with some loss of dentate granule neurons (Blümcke et al. 2013) (Fig. 3); thus we first confirmed the concordance of the clinical histopathological diagnosis with the degree of cell loss observed in our

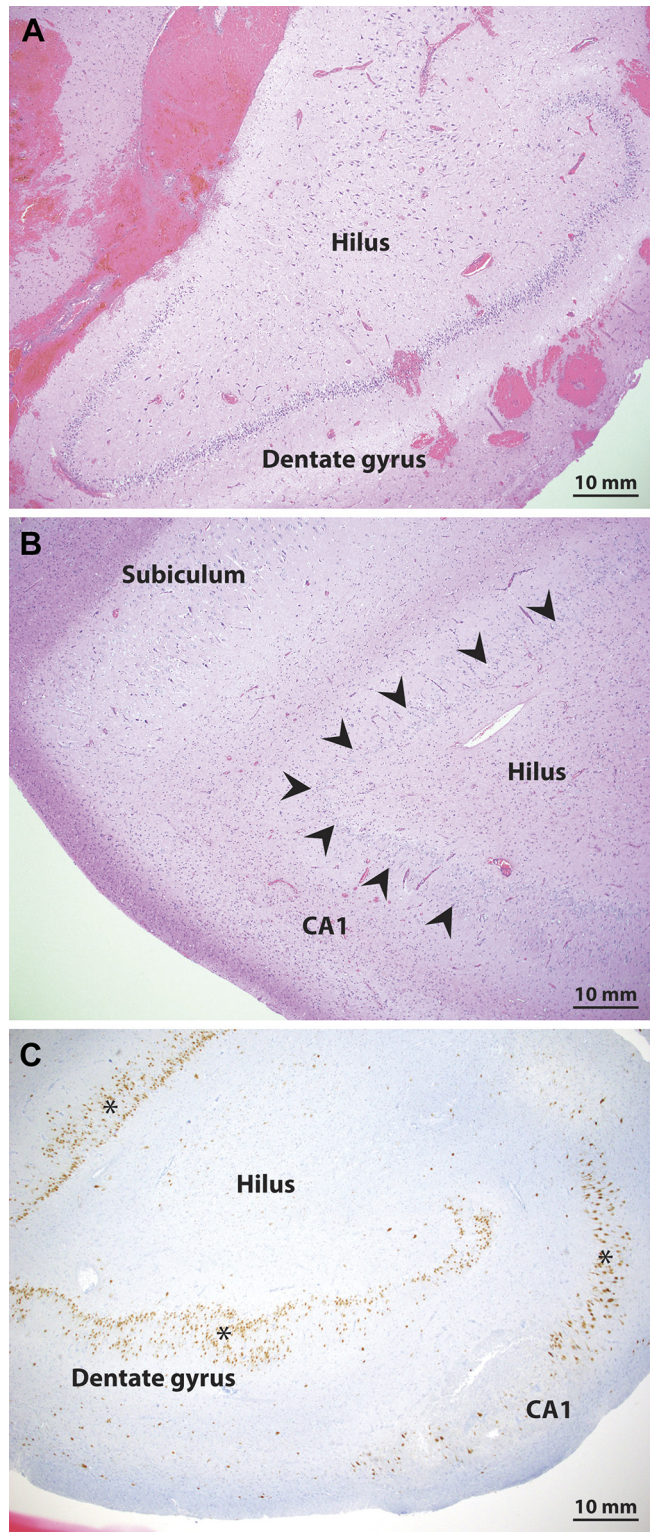

Fig. 3. Pathology confirmation of hippocampal sclerosis. *A* and *B*: hematoxylin and eosin stain staining shows preservation of the dentate granule cell layer in a nonsclerotic epilepsy patient (*A*) and clear cell loss in the dentate gyrus in a sample from a sclerotic epilepsy patient (*B*). *C*: additional staining with NeuN on an adjacent section from the sclerotic patient (highlighted with *) shows clear loss of neurons in the dentate gyrus and area CA1, consistent with the diagnosis of hippocampal sclerosis. Arrowheads mark the dentate granule cell layer in the sclerotic samples.

overall counts of dentate granule neurons. The number of dentate granule neurons per field was significantly different across the diagnosis groups ($F_{1,7}$: 11.4, $P = 0.006$) with the lowest density present in the sclerotic samples (12.2 ± 4.1 neurons/field) relative to control (36.7 ± 3.2 neurons/field) and nonsclerotic (30.4 ± 5.0 neurons/field) samples. Ad hoc testing revealed that only the sclerotic and the controls were significantly different (mean$\Delta = 24.7$, $P = 0.005$, Tukey–Kramer), indicating concordance with the clinical histopathological diagnoses.

Detection of GABA boutons in the nonepileptic human dentate granule cell layer. We next used multilabel fluorescence confocal microscopy to detect all GABA boutons in the dentate gyrus of human subjects without epilepsy, by labeling for vGAT, PV, GAD65, and GAD67 (Fig. 4, *A–D*). Colocalization of the different markers across the channels enabled the classification of different bouton subpopulations using mask operations. Three distinct subpopulations of vGAT boutons were identified based on GAD protein levels: vGAT+/GAD65+, vGAT+/GAD67+, and vGAT+/GAD65+/GAD67+. Specifically, vGAT+/GAD65+ boutons comprised 13.3 ± 4.8% of all vGAT+/GAD+ boutons, while vGAT+/GAD67+ and vGAT+/GAD65+/GAD67+ boutons accounted for 36.8 ± 11.6 and 49.9 ± 15.7%, respectively. Within the same samples, 18.9 ± 4.8% of vGAT+ boutons contained PV (vGAT+/PV+); 52.6 ± 17.4% of vGAT+/PV+ boutons contained both GAD65 and GAD67, while 47.4 ± 17.5% contained only GAD67. No vGAT+/PV+ boutons expressing GAD65 alone were observed. These findings, which quantify the vGAT+ population of the human hippocampus for the first time, are summarized in Fig. 5.

Detection of GABA bouton density differences in the epileptic dentate granule cell layer. We then evaluated the effect of MTLE on overall GABA bouton density (Fig. 4, *E–H*). Analysis of the density of vGAT+/GAD+ boutons per neuron showed a significant effect for the diagnosis group (control = 68.3 ± 7.4 boutons/neuron, nonsclerosis = 86.7 ± 25.2 boutons/neuron, and sclerosis = 129.5 ± 43.2 boutons/neuron; $F_{1,7} = 5.4$, $P = 0.04$). This effect was mediated by a 90% increase in vGAT+/GAD+ boutons/neuron in the sclerotic group when compared with the control group (mean$\Delta = 61.2$ bouton/neuron, $P = 0.03$).

To further assess potential differences in bouton density, the number of vGAT+/GAD+ boutons per volume of tissue was determined. There was a significant effect of diagnosis on vGAT+/GAD+ bouton density (control = 0.044 ± 0.0086 bouton/μm^3, nonsclerosis = 0.044 ± 0.0034 bouton/μm^3, and sclerosis = 0.021 ± 0.0032 bouton/μm^3; $F_{1,7} = 12.2$, $P = 0.005$) that was mediated by a 55% decrease in the sclerotic group compared with the control (mean$\Delta = 0.024$ bouton/μm^3, $P = 0.005$) and 52% decrease compared with the nonsclerotic (mean$\Delta = 0.023$ bouton/μm^3, $P = 0.02$) groups.

Next, the three vGAT+/GAD+ subpopulations were assessed independently. There was a trend for the vGAT+/GAD65+/GAD67+ subpopulation ($F_{1,7} = 7.2$, $P = 0.06$); however, no significant difference between the diagnosis groups was observed [vGAT+/GAD65+ ($F_{1,7} = 0.008$, $P = 0.9$) or vGAT+/GAD67+ ($F_{1,7} = 0.084$, $P = 0.9$)] (Fig. 6*A*). Additionally, the percentage of all vGAT+ boutons that each GAD subpopulation composed did not differ by diagnosis group [vGAT+/GAD65+ ($F_{1,7} = 2.21$, $P = 0.4$), vGAT+/GAD67+ ($F_{1,7} = 2.23$, $P = 0.4$), or vGAT+/GAD65+/GAD67+ ($F_{1,7} = 2.53$, $P = 0.4$)] (Fig. 6*B*). In summary, our findings suggest that in MTLE, perisomatic GABAergic innervation is increased on an individual granule cell neuron basis.

GABA-related protein levels in perisomatic boutons are highest in hippocampal sclerosis. Since bouton GAD and vGAT protein levels reflect a bouton's ability to synthesize and package GABA, respectively, we assayed the immunofluorescence levels of GAD and vGAT (Fig. 6, *C* and *D*) as a surrogate marker for relative protein levels in each of the three vGAT+/GAD+ subpopulations. Hippocampal sclerosis was associated with a greater amount of GAD immunofluorescence. GAD65 levels were approximately threefold higher in vGAT+/GAD65+ boutons ($F_{1,7} = 13.6$, $P = 0.02$) and twofold higher in vGAT+/GAD65+/GAD67+ boutons ($F_{1,7} = 23.1$, $P = 0.003$) relative to controls (Table 2). In sclerotic samples, vGAT+/GAD67+ bouton GAD67 immunofluorescence levels were more than twofold higher ($F_{1,7} = 15.7$, $P = 0.01$) but were unchanged in vGAT+/GAD65+/GAD67+ boutons ($F_{1,7} = 8.2$, $P = 0.06$) relative to controls (Table 2). The increased level of GAD immunofluorescence in the sclerotic group was associated with higher levels of vGAT bouton immunofluorescence levels (Table 2). In summary, inhibitory boutons exhibited an upregulation of the presynaptic machinery required for GABA transmission, suggesting that presynaptic inhibitory function is intact or possibly enhanced.

PV-expressing bouton alterations in MTLE. In the case of PV cells, we found that the PV+/GAD65+/GAD67+ and PV+/GAD67+ subpopulations were differentially affected in epilepsy. The density of PV+/GAD65+/GAD67+ boutons per neuron differed between diagnosis groups ($F_{1,7} = 14.5$, $P = 0.007$), which was mediated by a 266% increase in the sclerotic group compared with the control group (mean$\Delta = 16.6$ bouton/neuron, $P = 0.003$) and a 148% increase compared with the nonsclerotic group (mean$\Delta = 13.7$ bouton/neuron, $P = 0.02$) (Fig. 7). Similarly, PV+/GAD67+ bouton density showed a significant effect for the diagnosis group ($F_{1,6} = 16.4$, $P = 0.003$), but it was driven by a 75% decrease in density in the sclerotic group compared with the control group (Fig. 7). In terms of density per volume, PV+/GAD67+ boutons showed an effect for the diagnosis group ($F_{1,6} = 31.5$, $P = 0.0005$) with a 92% decrease in density in the sclerotic group (control = 0.0039 ± 0.00095 bouton/μm^3, nonsclerosis = 0.0032 ± 5.8e-05 bouton/μm^3, and sclerosis = 0.00031 ± 0.00012 bouton/μm^3). In contrast, there was a nonsignificant trend toward an increase in PV+/GAD65+/GAD67+ bouton density ($F_{1,7} = 0.5$, $P = 0.64$; Fig. 7).

We next assessed if PV bouton density varied across sampling regions. We found that the spatial distribution of vGAT+/PV+ bouton density across counting sites was more heterogeneous in sclerotic samples compared with the control samples (Fig. 7). The diagnosis group significantly affected the variance in PV bouton density across a single section (control: 19.6 ± 15.1 variance, nonsclerotic: 29.7 ± 9.4, and sclerotic: 249.6 ± 139.7; $F_{1,7} = 9.5$, $P = 0.01$) through greater variance in the sclerotic group compared with both groups. This heterogeneity was mediated by a change in PV+/GAD65+/GAD67+ bouton density variance (control: 8.9 ± 8.7 variance, nonsclerotic: 18.5 ± 7.6, and sclerotic: 227.4 ± 130.5; $F_{1,7} = 10$, $P = 0.009$), rather than PV+/GAD67+ bouton

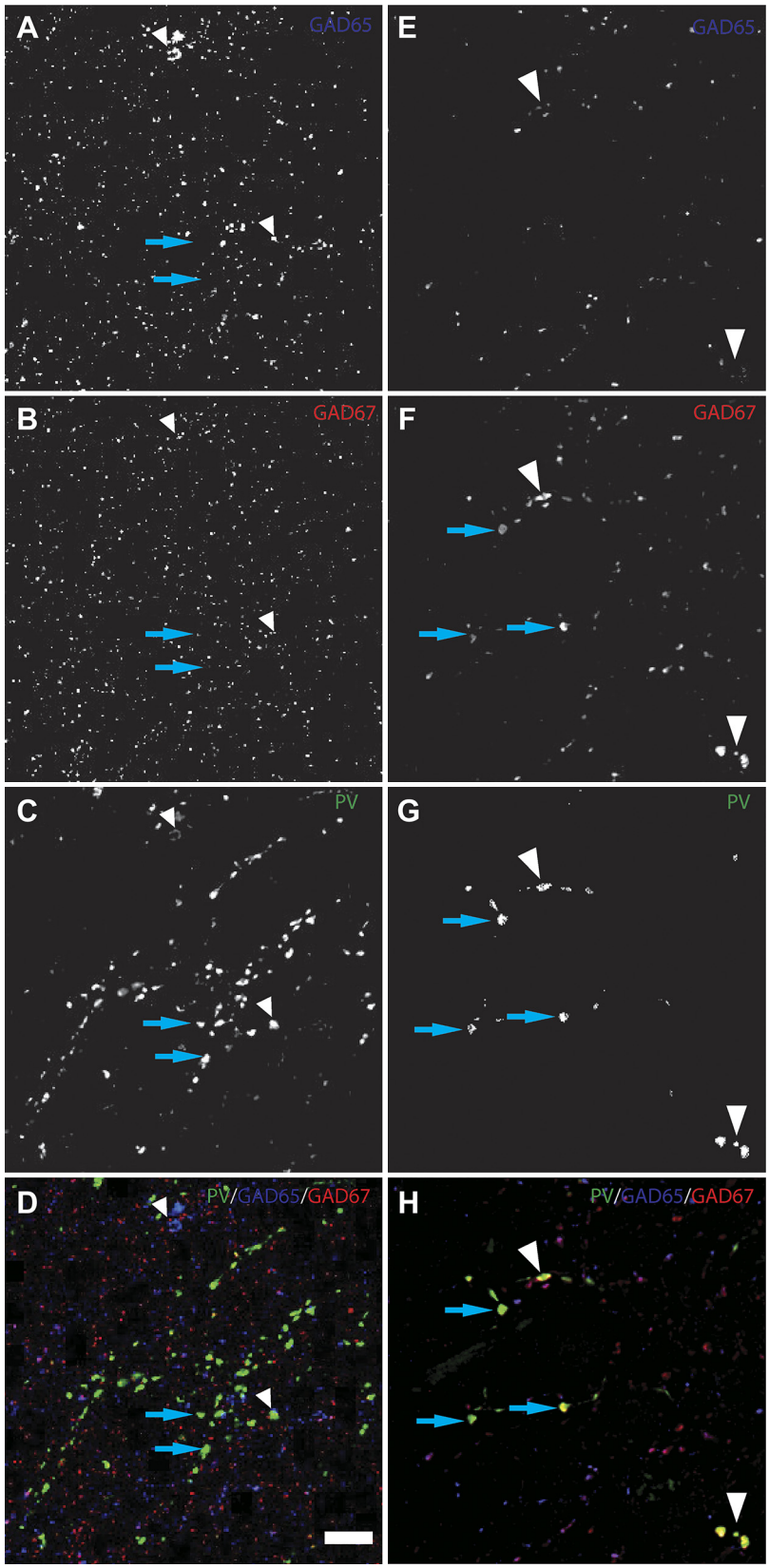

Fig. 4. *A–H*: immunofluorescence staining pattern in the human dentate granule layer in control (*A–D*) and sclerotic (*E–H*) samples. Deconvolved projection images of 5 *z*-planes are displayed for glutamic decarboxylase (GAD) 65 (*A* and *E*), GAD67 (*B* and *F*), parvalbumin (PV; *C* and *G*), and combined (*D* and *H*). White arrowheads represent identified PV+/GAD65+/GAD67+ boutons from presumed PV basket cells while blue arrows indicate PV+/GAD65-/GAD67+ boutons from presumed PV chandelier cells. Bar = 10 μm.

density variance, which did not differ across groups (control: 10.1 ± 10.4 variance, nonsclerotic: 7.7 ± 6.9, and sclerotic: 4.0 ± 3.2; $F_{1,7} = 0.5$, $P = 0.6$). The increase in variance is demonstrated in the distribution for each subtype across all sites (Fig. 8). There was a nonsignificant trend toward increased regional variability for all VGAT+ terminals in sclerotic samples (control: 442.7 ± 126.1 variance, nonsclerotic: 839.8 ± 438.8, and sclerotic: 6927 ± 6862; $F_{1,7} = 3.17$, $P = 0.1$).

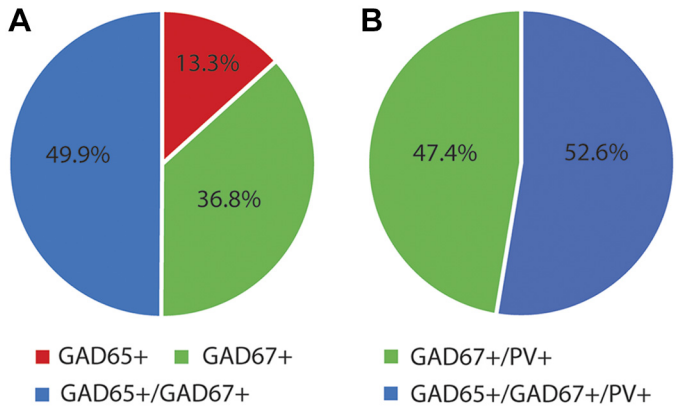

Fig. 5. Perisomatic inhibitory innervation of the normal human dentate granule cell layer. *A*: summary pie charts show vesicular GABA transporter-positive (vGAT+) bouton subpopulations based on glutamic decarboxylase (GAD) expression of which only 18.9 ± 4.8% of were also positive for parvalbumin (PV). *B*: the distribution of the PV+ boutons is summarized.

We next assessed vGAT, PV, GAD65, and GAD67 immunofluorescence levels in the two different PV bouton subpopulations. For PV+/GAD65+/GAD67+ boutons, we found an effect for the diagnosis group on GAD65 immunofluorescence level ($F_{1,6}$ = 46.0, P = 0.0007), GAD67 ($F_{1,7}$ = 25.0, P = 0.002), and vGAT ($F_{1,7}$ = 37.4, P = 7.3e-04) but not on PV itself ($F_{1,7}$ = 2.6, P = 0.37). Post hoc analysis revealed the same pattern for both GAD isoforms with GAD65 exhibiting a 440% increase and GAD67 exhibiting a 291% difference in the sclerotic group compared with controls (GAD65 meanΔ = 1,354 a.u., P = 0.000003; GAD67: meanΔ = 805 a.u., P = 0.0005), with 175% and 90% increase, respectively, compared with the nonsclerotic (GAD65 meanΔ = 1,057 a.u., P = 0.0005; GAD67: meanΔ = 514 a.u., P = 0.02) groups (Fig. 9*A*). Similarly, vGAT immunofluorescence level in the sclerotic group was significantly higher than in both the control (+356%, meanΔ = 904 a.u., P = 0.0002) and the nonsclerotic (+216%, meanΔ = 791 a.u., P = 0.002) groups.

For PV+/GAD67+ boutons, we found an effect for the diagnosis group on the immunofluorescence level of GAD67 ($F_{1,7}$ = 82.6, P = 0.00004), vGAT ($F_{1,7}$ = 51.0, P = 2.01e-04), and PV ($F_{1,7}$ = 11.8, P = 0.01). In post hoc analysis, the effect for GAD67 was mediated by an increase in the sclerotic group compared with both groups (control: +482%, meanΔ = 550 a.u., P = 0.00001; and nonsclerotic: +212%, meanΔ = 451 a.u., P = 0.0002) (Fig. 9*B*). vGAT demonstrated a similar pattern with increases in the sclerotic group of 400–500% increase in comparison with both the control (meanΔ = 679 a.u., P = 7.0e-5) and the nonsclerotic (meanΔ = 657 a.u., P = 3.6e-4) groups. However, the effect on PV was mediated by a 117% increase in the sclerotic group only when compared with the control group (meanΔ = 194 a.u., P = 0.005).

The above data suggest that significant changes in PV interneuron boutons in MTLE are specific to subjects with hippocampal sclerosis (Table 3). To further interpret these findings, we confirmed that similar to the prefrontal cortex, putative PVBCs in the human dentate gyrus express GAD65 and GAD67, but putative PVChCs only express GAD67. The granular layer of the dentate gyrus is extremely compact making it difficult to visualize PVChC cartridges. Out of several hundred images, only a handful of morphological cartridges were clearly recognizable (Fig. 10*A*). Therefore, we used fluorescence in situ hybridization and the recently identified ChC probe PTHLH (Fig. 10, *B* and *C*) to verify the identity of PVChCs. As shown in Fig. 10*D*, PTHLH+ neurons express GAD67, but not GAD65, a relationship that was present in all PTHLH+ nuclei, suggesting that in the human dentate gyrus, like the prefrontal cortex, PV+/GAD65+/GAD67+ boutons arise from PVBCs, while PV+/GAD67+ boutons arise from PVChCs.

DISCUSSION

In this proof-of-concept study, we used en bloc specimens from MTLE subjects with and without hippocampal sclerosis, paired with nonepileptic controls, to quantify the density of and synaptic protein content in boutons arising from two important interneuron populations, PVBCs and PVChCs. We developed a multilabel immunofluorescence confocal microscopy and custom segmentation algorithm capable of simultaneous quantitative assessment of bouton density, spatial distribution, relative immunofluorescence level, and structural features for multiple interneuronal subpopulations. We found that within

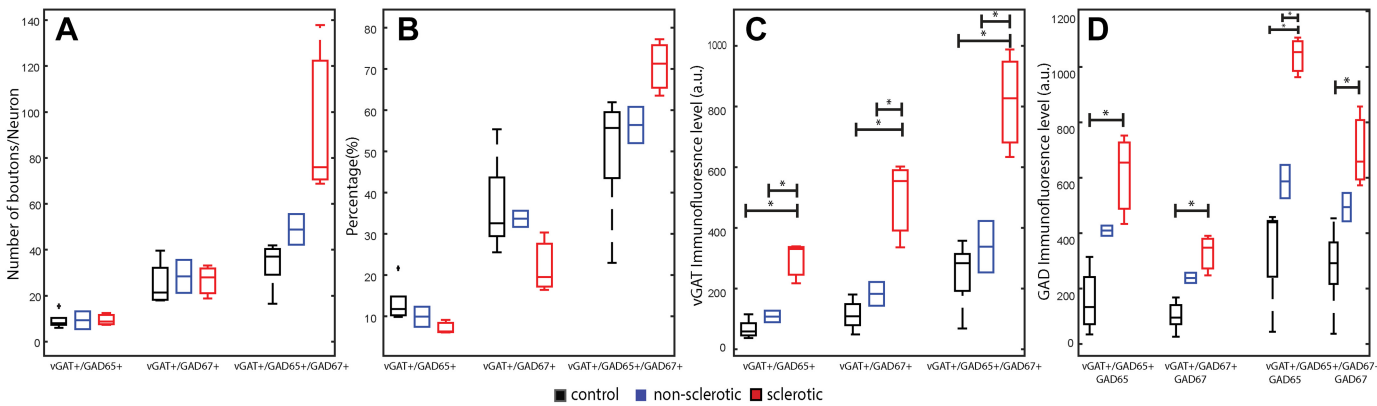

Fig. 6. Epilepsy-related changes in vesicular GABA transporter (vGAT)-immunoreactive bouton densities and immunofluorescence levels in the 3 glutamic decarboxylase (GAD) isoform combination subsets based on protein level. *A*: bouton density per neuron for all 3 subpopulations per diagnosis group. *B*: average percentage of each subpopulation relative to the total number of vGAT+ boutons. *C* and *D*: changes in protein level based on immunofluorescence are shown for vGAT protein level (*C*) and GAD isoform protein level (*D*). Boxplots are based on the average of all imaging sites per subject with the central mark representing the median in each group, and tails represent the 99th confidence interval; a.u. = arbitrary unit. Each diagnosis group was assigned a color: red: sclerosis; blue: nonsclerosis; black: control. *P < 0.05, significant interactions in post hoc analysis. $^{+}$Outlier values.

Table 2. *Inhibitory bouton protein expression changes in mesial temporal lobe epilepsy*

Bouton Population	*F* statistic	df	*P* value	Control vs. Sclerotic			Sclerotic vs. Nonsclerotic			Nonsclerotic vs. Control		
				MeanΔ	%Change	*P* value	MeanΔ	%Change	*P* value	MeanΔ	%Change	*P* value
vGAT protein expression, a.u.												
vGAT+/GAD65+	26.1	7	0.002	228	344	0.00005	187	176	0.006	41	NC	0.6
vGAT+/GAD67+	23.8	7	0.002	384	344	0.001	315	175	0.01	69	NC	0.6
vGAT+/GAD65+/GAD67+	23.1	7	0.003	477	230	0.01	567	143	0.002	89	NC	0.7
GAD protein expression, a.u.												
vGAT+/GAD65+	13.6	7	0.02	456	293	0.003	209	NC	0.2	252	NC	0.1
vGAT+/GAD67+	15.7	7	0.01	226	224	0.002	91	NC	0.3	137	NC	0.06
vGAT+/GAD65+/GAD67+ (GAD65)	23.1	7	0.003	701	208	0.00006	453	77	0.02	248	NC	0.2
vGAT+/GAD65+/GAD67+ (GAD67)	8.2	7	0.06	418	NC	0.01	204	NC	0.3	214	NC	0.2

vGAT, vesicular GABA transporter; GAD, glutamic decarboxylase; a.u., arbitrary units; NC, not calculated, as result did not reach significance after correction for multiple comparisons.

the dentate granule cell layer of subjects with hippocampal sclerosis, the density of PVBC boutons was increased, with only a trend toward a decrease in PVChC boutons, relative to matched nonepileptic comparison subjects. In contrast, these measures did not differ between epileptic subjects without sclerosis and matched comparison subjects. These results may explain conflicting findings from previous studies that have reported both preserved and lowered PV bouton densities, where technological limitations in conjunction with the scarcity of en bloc-resected tissue have precluded comprehensive assessments. In the future, this methodology can be used to study other interneuron populations, providing a framework for quantitative investigation of structural synaptic changes both in human epileptic tissue and animal models.

Perisomatic inhibitory innervation of the normal human dentate granule cell layer. We identified three vGAT-expressing bouton subpopulations in the human dentate granule cell layer based on GAD content, consistent with populations previously identified in the nonhuman primate and human prefrontal cortex (Fish et al. 2008, 2011; Glausier et al. 2014; Rocco et al. 2016b), including two subpopulations of PV boutons: those expressing GAD67 only (PVChCs) and those expressing both GAD67 and GAD65 (PVBCs) (Fish et al. 2011; Glausier et al. 2014). Boutons from PV cells accounted for nearly 19% of all perisomatic inhibitory boutons, which is consistent with the 16–29% range reported in a previous human hippocampal electron microscopy study (Wittner et al. 2005).

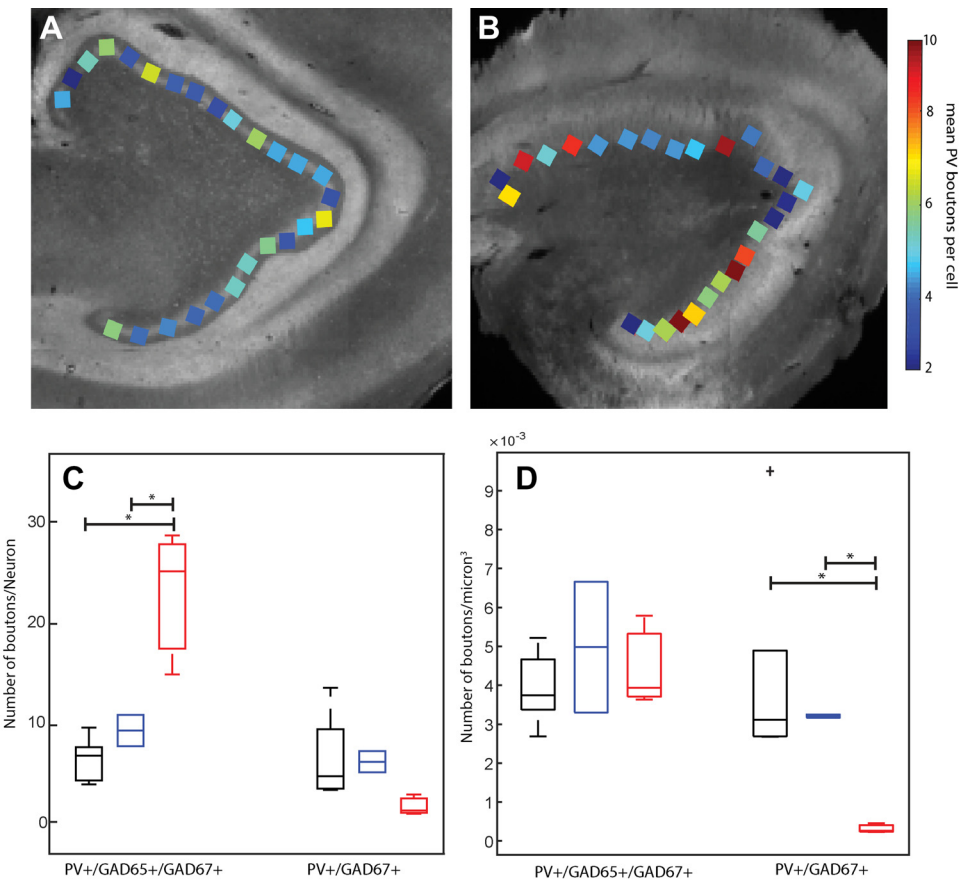

Fig. 7. Epilepsy-related changes in parvalbumin (PV)-immunoreactive bouton densities and spatial distribution. *A* and *B*: the spatial distribution of total PV+ bouton density per neuron is represented by mapping the density value in each imaging field to its location on the montage image for a control subject (*A*) and his age- and sex-matched sclerotic subject (*B*). *C* and *D*: boxplots represent PV basket cells (*C*) and PV chandelier cells (*D*) bouton density across the diagnosis groups based on the average of all imaging sites per subject with the central mark representing the mean in each group, and tails represent the 99th confidence interval; a.u. = arbitrary unit. Each diagnosis group was assigned a color: red: sclerosis; blue: nonsclerosis; black: control. *$P < 0.05$, significant interactions in post hoc analysis. $^{+}$Outlier values.

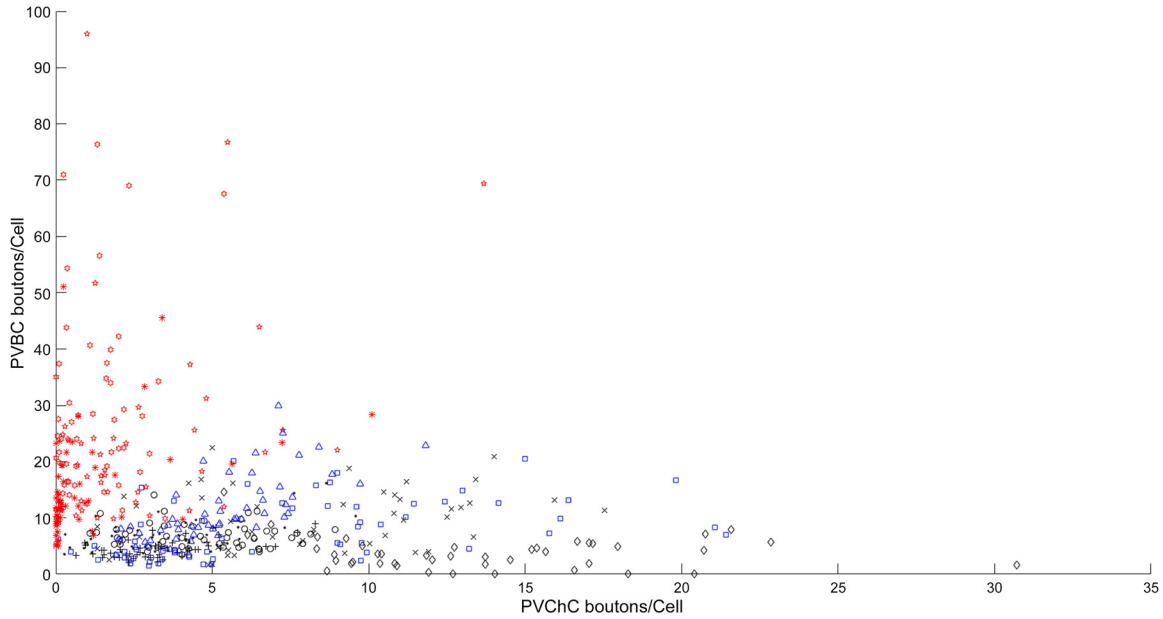

Fig. 8. Distribution of parvalbumin (PV) basket cells (PVBCs) and PV chandelier cell (PVChC) innervation in the dentate gyrus. Scatterplot showing the density of PVBC and PVChC boutons per dentate granule neuron at an imaging site. Each study subject was assigned a unique symbol with the color representing the diagnostic group (red: sclerosis; blue: nonsclerosis; black: control).

Structural upregulation of inhibitory components in MTLE with sclerosis. Since a seminal report demonstrating preserved inhibitory innervation following perforant path stimulation-induced epilepsy in rodents (Sloviter 1987), several studies have provided similar evidence suggesting that perisomatic innervation is preserved in both nonsclerotic and sclerotic MTLE (Arellano et al. 2004; Bausch 2005; Mathern et al. 1995; Wittner et al. 2001, 2002; Zhang et al. 2009a, 2009b). In contrast, findings from other studies suggest that GABA bouton density is decreased in sclerotic MTLE (Andrioli et al. 2007; Arellano et al. 2004; Sloviter et al. 1991; Wittner et al. 2001). Across these studies, overall immunoreactivity across a volume was reduced. This observation was recapitulated in our finding that vGAT+ bouton density per volume of tissue (number/μm^3) was decreased by ~50% in sclerotic epilepsy compared with subjects without sclerosis or controls. However, these values do not take into account the effects of sclerosis, cell loss, or dispersion seen in MTLE. While one previous study using electron microscopy to examine inhibitory input on a per neuron level reported preservation of bouton density (Wittner et al. 2001), we observed that the number of vGAT+ boutons per dentate granule neuron was ~90% greater in subjects with sclerosis. Thus, despite the known loss of GABAergic cells in MTLE (Andrioli et al. 2007; Arellano et al. 2004; Sloviter et al. 1991; Wittner et al. 2001), dentate granule neurons appear to receive a greater number of GABA inputs in the setting of sclerosis, suggesting that the structural substrates for perisomatic inhibition in the dentate granule cell layer may be enhanced. Interestingly, nonsclerotic epilepsy patients were differentiated clinically from those with sclerosis by having much more frequent seizures, which also could affect these results.

Although immunofluorescence is not a direct measure of protein content, as the antibody binding can be affected by a host of tissue factors, our samples were processed simultaneously and in an identical manner to minimize differences. Furthermore, we normalized all immunofluorescence levels to correct for differences in exposure time across samples. Therefore, the relative difference in immunofluorescence observed in these data reasonably can be used to infer differences in protein content. Our quantitative immunofluorescence approach suggests that GABA boutons contain more GAD65, GAD67, and vGAT protein levels in sclerotic samples. Bouton levels of GAD65 immunofluorescence were twice as high as levels of GAD67. GAD67 accounts for the majority of GABA synthesis in the cortex (Battaglioli et al. 2003; Mason et al. 2001), but GAD67 alone is unable to support the high-efficiency reloading of GABA vesicles required for normal function during conditions of high demand (Kleppner and Tobin 2002). In fact, GAD65 synthesis is highly regulated in response to GABA concentration and neuronal activity, while very little regulation is placed on GAD67 synthesis (Kleppner and Tobin 2002). In the epileptic dentate gyrus, therefore, increased excitatory network activity may induce a compensatory mechanism that manifests as sharp increases in GAD65 protein at the bouton level.

Parvalbumin-interneuron derangement in MTLE. Our focus on PV+ interneurons comes from their well-documented neurophysiological significance in orchestrating hippocampal theta, gamma, and ripple oscillatory activity in the normal rodent brain (Freund and Buzsáki 1996; Klausberger and Somogyi 2008; Somogyi et al. 1982), their impaired development or function in various animal models of epilepsy (Jiang et al. 2016), and their vulnerability in human epilepsy (Andrioli et al. 2007; Arellano et al. 2004; Sloviter et al. 1991; Wittner et al. 2001, 2005). In sclerotic samples, where PV cells are especially vulnerable, we observed a 75% decrease in PVChC boutons, both in terms of absolute volumetric density and density relative to the number of dentate granule neurons. In contrast, prior studies have reported increased chandelier cartridge complexity (Arellano et al. 2004) and increased PV+ inhibitory synapses on granule cell axon initial segments (Witt-

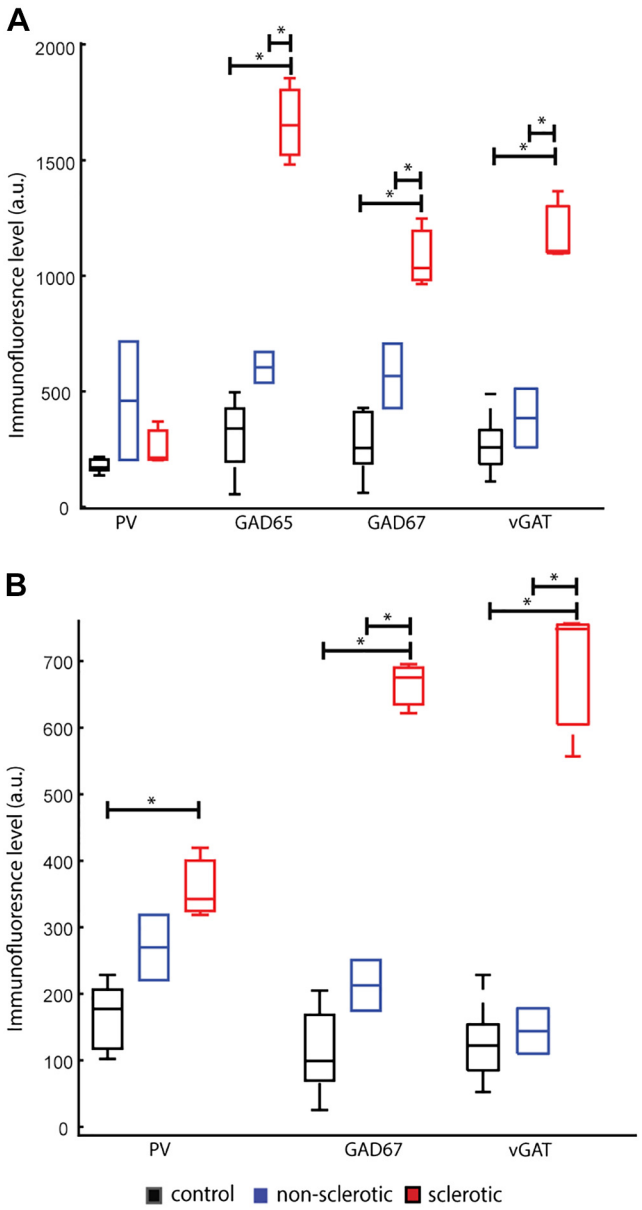

Fig. 9. Epilepsy-related increase in parvalbumin (PV)-immunoreactive bouton immunofluorescence levels. *A* and *B*: boxplots representing PV basket cell bouton protein level profile across the diagnostic groups (*A*) as measured by the immunofluorescence of PV, glutamic decarboxylase (GAD) 65, GAD67, and vesicular GABA transporter (vGAT) and PV chandelier cell bouton protein level profile across the diagnostic groups (*B*) as measured by the immunofluorescence of PV, GAD67, and vGAT. Boxplots are based on the average of all imaging sites per subject with the central mark representing the median in each group, tails represent the 99th confidence interval; a.u. = arbitrary unit. Each diagnosis group was assigned a color: red: sclerosis; blue: nonsclerosis; black: control. $*P < 0.05$, significant interactions in post hoc analysis.

ner et al. 2001). However, these prior observations were made within regions with intact PV innervation, rather than averaging across the entire dentate granule cell layer as reported here to account for the expanses devoid of PV boutons. Therefore, while a small number of dentate granule neurons might receive an increase in PVChC input, the overall coverage by PVChCs is decreased selectively. Of note, the preserved PVChC input reported by Wittner et al. (2001) is based on finding putative inhibitory synapses on dentate granule neuron AIS that are PV negative and failed to stain for NPY, CCK, or SOM. Those investigators concluded that PV protein level might be lost in a subset of boutons; however, they also reported increased immunoreactivity in preserved boutons, similar to our findings. In another interpretation, the PV-negative cartridges may represent calbindin cartridges, which have been reported to be increased selectively in sclerotic samples (Arellano et al. 2004). We acknowledge that no counterstaining for the AIS was performed to determine whether the observed loss of PV+ GABAergic synapses from chandelier cells might be driven by structural/functional alterations in the AIS.

Due to the high resolution of our microscopy technique, we interpret the loss of PV boutons as a result of the loss of the PV cells from which they originate, rather than loss of immunogenicity of present boutons. We acknowledge, however, that the absence of PV staining does not necessarily indicate cell or bouton loss (Sloviter et al. 1991). Although PVChCs represent a small portion of the inhibitory interneuron population, each PVChC innervates hundreds to thousands of dentate granule neurons (DeFelipe 1999), suggesting they can exert substantial inhibitory control through their privileged input on the axon initial segment (Buhl et al. 1994; Miles et al. 1996). These properties may allow PVChCs to act as network-wide switches to prevent hyperexcitability (Zhu et al. 2004) but also may lead to widespread effects when even a small number of PVChCs are lost. For instance, it has been suggested that the loss of PVChCs could result in the generation of microcircuits that permit runaway excitation and the propagation of seizure activity (Zhu et al. 2004).

In contrast, PVBCs exhibited a 250% increase in perisomatic input onto dentate granule neurons, suggesting a different intrinsic response to the disease state. The increase in PVBC input was heterogeneous across the dentate granule cell layer, accounting for the increase in PV innervation variance. Patchy changes in PV boutons have been described previously in hippocampal sclerosis, but these reports did not provide data from nonsclerotic and nonepileptic control samples (Andrioli et al. 2007; Arellano et al. 2004; Sloviter et al. 1991; Wittner et al. 2001, 2005). Increased PVBC input in the dentate granule cell layer may reflect a compensatory mechanism for the loss of PVChC boutons, although enhanced input does not necessarily reflect beneficial inhibitory changes, as pathological hypersynchrony may occur through the creation of neuronal ensembles containing more dentate granule neuron being coordinated by the same PVBCs (Babb et al. 1989; Bragin et al. 2000; Ellender et al. 2014). While PVBCs are essential for maintaining ripple oscillations, coordinated inhibitory interneuron activity also has been implicated as the generator of pathological ripples that can drive epileptiform activity (Bragin et al. 1999) and act as a marker for epileptogenic tissue (Worrell and Gotman 2011). It is possible, therefore, that PVBCs could facilitate the generation of epileptiform activity in the setting of PVChC loss.

In addition to the differential structural alterations in PVBCs and PVChCs, GAD and vGAT protein content in individual boutons was higher for both PV subpopulations. While the relative GAD67 protein levels were similarly higher between the two interneuron types, PVBC boutons exhibited relatively greater GAD65 protein levels (440 vs. 175%). This marked increase in GAD65 levels suggests that the demands of increased network activity in epilepsy surpass the compensatory

Table 3. *Summary of significant findings*

	t-Statistic							
	Nonsclerotic				Sclerotic			
Interneuron Types	Density (per DGN)	vGAT	GAD65	GAD67	Density (per DGN)	vGAT	GAD65	GAD67
PV GAD65+/67+ (basket cell)	n.s.	n.s.	n.s.	n.s.	↑ ↑ ↑	↑ ↑ ↑ ↑	↑ ↑ ↑ ↑	↑ ↑ ↑
PV GAD67+ (chandelier cell)	n.s.	n.s.	n.a.	n.s.	↓	↑ ↑ ↑ ↑	n.a.	↑ ↑ ↑ ↑
nonPV GAD65+/67+	n.s.	n.s.	n.s.	n.s.	↑	↑ ↑	n.s.	n.s.
nonPV GAD67+	n.s.	n.s.	n.a.	↑ ↑	n.s.	↑ ↑ ↑ ↑	n.a.	↑ ↑ ↑
nonPV GAD65+	n.s.	n.s.	↑ ↑	n.a.	n.s.	↑ ↑ ↑ ↑	↑ ↑ ↑	n.a.

PV, parvalbumin; vGAT, vesicular GABA transporter; GAD, glutamic decarboxylase; DGN, dentate granule neurons. ↑ = Up to 1-fold; ↑ ↑ = 1- to 2-fold; ↑ ↑ ↑ = 2- to 3-fold; ↑ ↑ ↑ ↑ = > 3-fold; n.a., not applicable; n.s., not significant.

GABA response achievable through GAD67 regulation, as GAD67 protein level itself was tripled. These findings suggest that PV interneurons respond to enhanced excitatory input (Wittner et al. 2001) by increasing their inhibitory output.

Functional consequences of the structural inhibitory changes. The functional consequences of these structural changes are far more complicated than simply increased or decreased inhibition and several caveats need to be considered when interpreting these data. While we mapped perisomatic innervation, we did not explore other sources of inhibitory control, such as dendritic inhibitory input (Cossart et al. 2001). Efficient GABA transmission also depends on the release probability of vesicles (Hirsch et al. 1999) and postsynaptic molecular machinery, including changes that may lead to paradoxical depolarization (Bausch 2005). Additionally, loss of PVChC boutons may outweigh any enhanced perisomatic inputs, due to their privileged location on the axon initial segment. These contrasting effects on different modes of inhibitory input could potentially explain previous findings in the literature suggesting that both diminished and enhanced aspects of inhibition are present (Cossart et al. 2001; Esclapez et al. 1997; Isokawa-Akesson et al. 1989; Kobayashi and Buckmaster 2003; Löscher 2011; Prince and Jacobs 1998; Williamson et al. 1999; Zhang and Buckmaster 2009).

Technical considerations. Structural imaging of axonal boutons can differentiate between interneuron subtypes based on their neurochemical protein levels, and morphological features often correlate with changes in the functional properties of

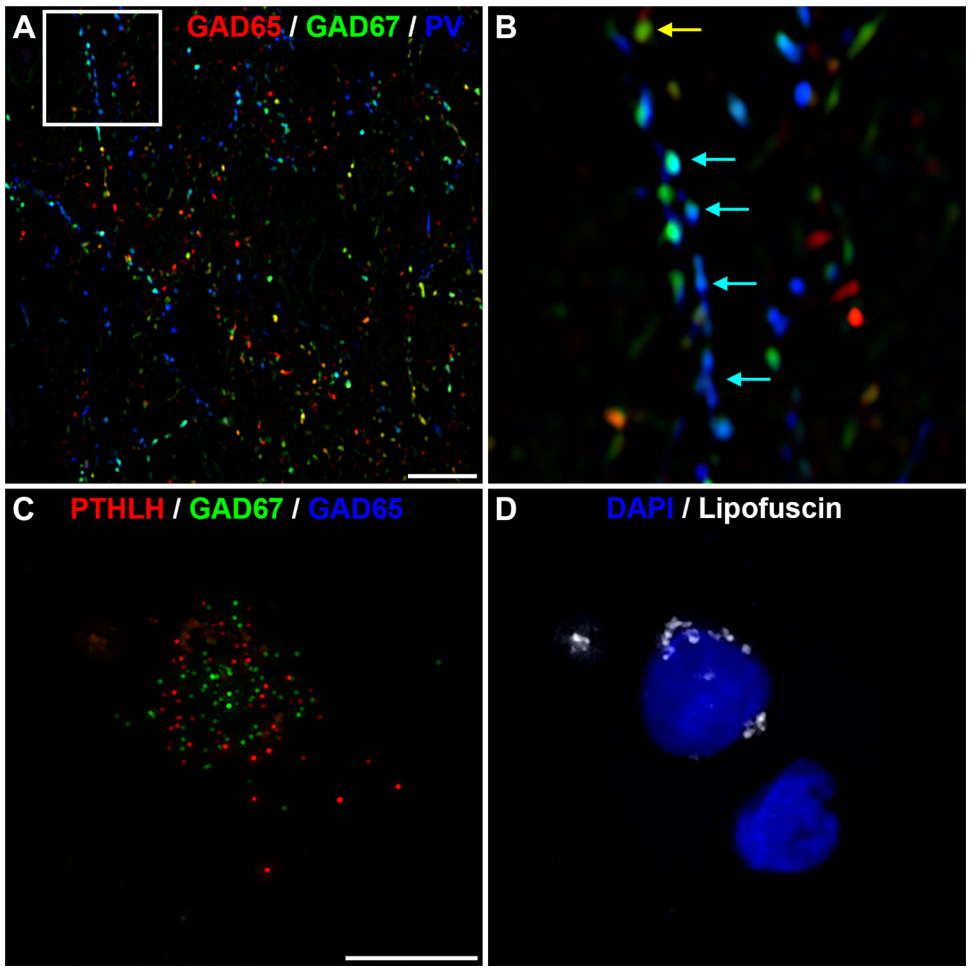

Fig. 10. Parvalbumin (PV) chandelier cells expressed glutamic decarboxylase (GAD) 67 but not GAD65 in the human dentate gyrus. *A* and *B*: labeling of PV terminals in human dentate gyrus demonstrating that ChC cartridge boutons contain GAD67 but not GAD65. *B*: ×4 magnification of the boxed region in *A*. *C* and *D*: PTHLH/GAD65/GAD67 multiplex RNAscope. DAPI and lipofuscin were imaged in a 4th and 5th channel. Note the absence of GAD65 mRNA grains. Bars = 10 μm.

synapses (Pierce and Lewin 1994). The traditional standard method for reliable identification of a cell-type specific synapse is immunoelectron microscopy. This approach, however, is costly and prohibitively slow for assessing large areas of tissue, as is required for determining the density of PVBC and PVChC boutons in relation to principal neuron density throughout the dentate gyrus in epilepsy. In addition, no previous studies have explored whether compensatory changes in the ability of PVBC and PVChC boutons to synthesize and release GABA are present in epilepsy, which would be difficult to assess by immunoelectron microscopy, since this technique offers only limited molecular discrimination (Simhal et al. 2017). Performing fluorescence intensity measures in human cortex, however, can be challenging due to both fixative-induced fluorescence and native fluorescence (e.g., from lipofuscin) (Benavides et al. 2002; Porta 2002). We took several steps to address this issue ranging from simply pretreating sections with 1% sodium borohydride to reduce fixative-induced fluorescence (Clancy and Cauller 1998; Mukherji et al. 1966) to developing a robust algorithm to detect and mask lipofuscin, a major source of native fluorescence in human tissue (Curley et al. 2011; Glausier et al. 2014; Moyer et al. 2012, 2013; Rocco et al. 2016a, 2017). In addition to dealing with tissue autofluorescence, measures of protein in postmortem human tissue are subject to the potential confound of PMI and storage time (Beneyto et al. 2009). While surgical tissue is fixed immediately after removal, removal is preceded by 1–2 h of vascular disconnection thus representing its true PMI. Additionally, the only source of control hippocampi is postmortem tissue. However, the effect of PMI on antigenicity is variable (little to no effect on the detectability of some proteins but large effects on others). To that end, we have shown in numerous studies using different techniques, Western blots and densitometry, that the proteins measured in this study are stable across PMIs reaching up to 20 h. Additionally, storage time showed little to no effect on their levels (Curley et al. 2011; Glausier et al. 2015; Moyer et al. 2012; Rocco et al. 2016a). We even went further to show stability compared with a true PMI of 0 from nonhuman primate tissue (Curley et al. 2011). Finally, while the nonsclerotic and sclerotic samples shared near identical PMIs and storage times in our cohort, the protein levels of the nonsclerotic samples nearly matched those of the postmortem controls used here suggesting that PMI did not play a significant effect on the results. Nonetheless, to control for any potential effects of PMI and storage time, these values were included as covariates in the statistical analysis.

In the current study, we applied this method to image the human dentate gyrus for the first time at the level of boutons. The limitations of our approach are mostly confined to the signal to background ratio. That is, puncta of very low fluorescence intensities are difficult to mask because their signal to background ratios are very small. However, the iterative segmentation algorithm ensures masking all puncta regardless of fluorescence levels as shown on both real and simulated data (Fish et al. 2008). Additionally, while fluorescence labeling is highly correlated with higher resolution imaging through electron microscopy (Robinson and Takizawa 2009), its ability to resolve neighboring fluorescent objects is hindered by the PSF of the fluorescent source. However, the combination of deconvolution and three-dimensional Gaussian subtraction to greatly reduce the effects of PSF and the use of size gating based on synaptic measurements from electron microscopy literature allows us to resolve single boutons (Fish et al. 2008). Finally, the robust ability of this technique to detect surrogate protein level changes specific to neuronal subtypes that would not be detected through traditional approaches has been demonstrated in numerous publications, including confirmation by independent measures such as RNAscope (Curley et al. 2011; Fish et al. 2008, 2011; Glausier et al. 2014, 2015; Moyer et al. 2012, 2013; Rocco et al. 2016a, 2016b, 2017; Sweet et al. 2010). In this study, our method was applied to assess protein levels in synaptic boutons of neuronal subtypes that sometimes represent $<10\%$ of overall boutons, which would not be possible with techniques such as Western blot.

We acknowledge that the identification of PV+/GAD67+ boutons as chandelier cell boutons is not absolute. Nonetheless, recent work from the Allen Institute using single nucleus RNA sequencing data from PV cells in the human middle temporal gyrus identified that a highly distinctive PV type (Inh L2–5 PVALB SCUBE3) likely corresponds to chandelier (axo-axonic) cells (Hodge et al. 2019). Data from the Allen Brain Atlas (https://celltypes.brain-map.org/rnaseq/human/cortex) indicate that these cells express PTHLH and GAD1 (the gene for Gad67) but not GAD2 (the gene for GAD65), supporting our use of PTHLH to confirm the axo-axonic identity of PV+GAD67+ cells in our samples. Importantly, the findings from Hodge et al. (2019) reinforce a major impetus for the current work: despite a general conservation, extensive differences between homologous human and mouse cell types (marked alterations in proportions, laminar distributions, gene expression, and morphology) demonstrate how critical it is to study the human brain directly.

Conclusions. This proof-of-concept study establishes a new methodology for bouton-level investigation of the human hippocampus. Although the sample size is small, no previous histological study has matched en bloc resected nonsclerotic and sclerotic human MTLE specimens to those from age-matched controls. The functional consequences of the structural changes we observed are more complicated than simply increased or decreased inhibition, and we did not explore the effects of MTLE on postsynaptic molecular machinery, including changes that may lead to paradoxical depolarization (Bausch 2005). Nonetheless, since sclerotic and nonsclerotic MTLE patients can share the same clinical syndrome in terms of seizure type and severity, and nonsclerotic hippocampi did not display significant differences compared with controls in the majority of assayed parameters, the data may reflect mechanisms through which seizure severity increases or cognitive function decreases. Indeed, the detail provided by this new method may reflect one of multiple substantial cellular changes that ultimately support recurrent, pathological neuronal synchronization in the injured circuit. Despite the fact that studies of en bloc human hippocampal resections following epilepsy surgery are becoming exceedingly rare, the application of these techniques in larger cohorts of human specimens should be undertaken, including closer evaluation of the 80% of interneuron boutons that do not contain PV.

ACKNOWLEDGMENTS

We appreciate the generous gift of control tissue from Dr. David Lewis.

GRANTS

Funding was provided by the Walter L. Copeland Fund of The Pittsburgh Foundation (to R. M. Richardson) and National Center for Advancing Translational Sciences Grant UL1-TR-0000005 (to R. M. Richardson and K. N. Fish).

DISCLOSURES

No conflicts of interest, financial or otherwise, are declared by the authors.

AUTHOR CONTRIBUTIONS

K.N.F., T.A.W., and R.M.R. conceived and designed research; .A., K.N.F., V.S., and R.L.H. performed experiments; A.A., K.N.F., and T.A.W. analyzed data; A.A., K.N.F., T.A.W., V.S., and R.M.R. interpreted results of experiments; A.A. and R.M.R. prepared figures; A.A. drafted manuscript; A.A., K.N.F., T.A.W., R.L.H., and R.M.R. edited and revised manuscript; A.A., K.N.F., and R.M.R. approved final version of manuscript.

REFERENCES

Andrioli A, Alonso-Nanclares L, Arellano JI, DeFelipe J. Quantitative analysis of parvalbumin-immunoreactive cells in the human epileptic hippocampus. *Neuroscience* 149: 131–143, 2007. doi:10.1016/j.neuroscience.2007.07.029.

Arellano JI, Muñoz A, Ballesteros-Yáñez I, Sola RG, DeFelipe J. Histopathology and reorganization of chandelier cells in the human epileptic sclerotic hippocampus. *Brain* 127: 45–64, 2004. doi:10.1093/brain/awh004.

Babb TL, Pretorius JK, Kupfer WR, Crandall PH. Glutamate decarboxylase-immunoreactive neurons are preserved in human epileptic hippocampus. *J Neurosci* 9: 2562–2574, 1989. doi:10.1523/JNEUROSCI.09-07-02562.1989.

Battaglioli G, Liu H, Martin DL. Kinetic differences between the isoforms of glutamate decarboxylase: implications for the regulation of GABA synthesis. *J Neurochem* 86: 879–887, 2003. doi:10.1046/j.1471-4159.2003.01910.x.

Bausch SB. Axonal sprouting of GABAergic interneurons in temporal lobe epilepsy. *Epilepsy Behav* 7: 390–400, 2005. doi:10.1016/j.yebeh.2005.07.019.

Benavides SH, Monserrat AJ, Fariña S, Porta EA. Sequential histochemical studies of neuronal lipofuscin in human cerebral cortex from the first to the ninth decade of life. *Arch Gerontol Geriatr* 34: 219–231, 2002. doi:10.1016/S0167-4943(01)00223-0.

Beneyto M, Sibille E, Lewis DA. Human postmortem brain research in mental illness syndromes. In: *Neurobiology of Mental Illness*, edited by Charney D, Nestler E. New York: Oxford University Press, 2009, p. 202–214.

Bezchlibnyk YB, Willie JT, Gross RE. A neurosurgeon's view: Laser interstitial thermal therapy of mesial temporal lobe structures. *Epilepsy Res* 142: 135–139, 2018. doi:10.1016/j.eplepsyres.2017.10.015.

Blümcke I, Thom M, Aronica E, Armstrong DD, Bartolomei F, Bernasconi A, Bernasconi N, Bien CG, Cendes F, Coras R, Cross JH, Jacques TS, Kahane P, Mathern GW, Miyata H, Moshé SL, Oz B, Özkara Ç, Perucca E, Sisodiya S, Wiebe S, Spreafico R. International consensus classification of hippocampal sclerosis in temporal lobe epilepsy: a Task Force report from the ILAE Commission on Diagnostic Methods. *Epilepsia* 54: 1315–1329, 2013. doi:10.1111/epi.12220.

Bragin A, Engel J Jr, Wilson CL, Fried I, Mathern GW. Hippocampal and entorhinal cortex high-frequency oscillations (100–500 Hz) in human epileptic brain and in kainic acid-treated rats with chronic seizures. *Epilepsia* 40: 127–137, 1999. doi:10.1111/j.1528-1157.1999.tb02065.x.

Bragin A, Wilson CL, Engel J Jr. Chronic epileptogenesis requires development of a network of pathologically interconnected neuron clusters: a hypothesis. *Epilepsia* 41, *Suppl* 6: S144–S152, 2000. doi:10.1111/j.1528-1157.2000.tb01573.x.

Buhl EH, Halasy K, Somogyi P. Diverse sources of hippocampal unitary inhibitory postsynaptic potentials and the number of synaptic release sites. *Nature* 368: 823–828, 1994. [Erratum in *Nature* 387: 106, 1997.] doi:10.1038/368823a0.

Celio MR, Baier W, Schärer L, de Viragh PA, Gerday C. Monoclonal antibodies directed against the calcium binding protein parvalbumin. *Cell Calcium* 9: 81–86, 1988. doi:10.1016/0143-4160(88)90027-9.

Chaudhry FA, Reimer RJ, Bellocchio EE, Danbolt NC, Osen KK, Edwards RH, Storm-Mathisen J. The vesicular GABA transporter, VGAT, localizes to synaptic vesicles in sets of glycinergic as well as GABAergic neurons. *J Neurosci* 18: 9733–9750, 1998. doi:10.1523/JNEUROSCI.18-23-09733.1998.

Chen Z, Brodie MJ, Liew D, Kwan P. Treatment outcomes in patients with newly diagnosed epilepsy treated with established and new antiepileptic drugs: a 30-year longitudinal cohort study. *JAMA Neurol* 75: 279–286, 2018. doi:10.1001/jamaneurol.2017.3949.

Clancy B, Cauller LJ. Reduction of background autofluorescence in brain sections following immersion in sodium borohydride. *J Neurosci Methods* 83: 97–102, 1998. doi:10.1016/S0165-0270(98)00066-1.

Cossart R, Dinocourt C, Hirsch JC, Merchan-Perez A, De Felipe J, Ben-Ari Y, Esclapez M, Bernard C. Dendritic but not somatic GABAergic inhibition is decreased in experimental epilepsy. *Nat Neurosci* 4: 52–62, 2001. doi:10.1038/82900.

Curley AA, Arion D, Volk DW, Asafu-Adjei JK, Sampson AR, Fish KN, Lewis DA. Cortical deficits of glutamic acid decarboxylase 67 expression in schizophrenia: clinical, protein, and cell type-specific features. *Am J Psychiatry* 168: 921–929, 2011. doi:10.1176/appi.ajp.2011.11010052.

DeFelipe J. Chandelier cells and epilepsy. *Brain* 122: 1807–1822, 1999. doi:10.1093/brain/122.10.1807.

DeFelipe J, Hendry SH, Jones EG, Schmechel D. Variability in the terminations of GABAergic chandelier cell axons on initial segments of pyramidal cell axons in the monkey sensory-motor cortex. *J Comp Neurol* 231: 364–384, 1985. doi:10.1002/cne.902310307.

Dudek FE, Sutula TP. Epileptogenesis in the dentate gyrus: a critical perspective. *Prog Brain Res* 163: 755–773, 2007. doi:10.1016/S0079-6123(07)63041-6.

Dumitriu D, Berger SI, Hamo C, Hara Y, Bailey M, Hamo A, Grossman YS, Janssen WG, Morrison JH. Vamping: stereology-based automated quantification of fluorescent puncta size and density. *J Neurosci Methods* 209: 97–105, 2012. doi:10.1016/j.jneumeth.2012.05.031.

Ellender TJ, Raimondo JV, Irkle A, Lamsa KP, Akerman CJ. Excitatory effects of parvalbumin-expressing interneurons maintain hippocampal epileptiform activity via synchronous afterdischarges. *J Neurosci* 34: 15208–15222, 2014. doi:10.1523/JNEUROSCI.1747-14.2014.

Esclapez M, Hirsch JC, Khazipov R, Ben-Ari Y, Bernard C. Operative GABAergic inhibition in hippocampal CA1 pyramidal neurons in experimental epilepsy. *Proc Natl Acad Sci USA* 94: 12151–12156, 1997. doi:10.1073/pnas.94.22.12151.

Faraji AH, Richardson RM. New antiepileptic drugs have not improved treatment outcomes. *Neurosurgery* 82: E99, 2018. doi:10.1093/neuros/nyy053.

Fish KN, Hoftman GD, Sheikh W, Kitchens M, Lewis DA. Parvalbumin-containing chandelier and basket cell boutons have distinctive modes of maturation in monkey prefrontal cortex. *J Neurosci* 33: 8352–8358, 2013. doi:10.1523/JNEUROSCI.0306-13.2013.

Fish KN, Sweet RA, Deo AJ, Lewis DA. An automated segmentation methodology for quantifying immunoreactive puncta number and fluorescence intensity in tissue sections. *Brain Res* 1240: 62–72, 2008. doi:10.1016/j.brainres.2008.08.060.

Fish KN, Sweet RA, Lewis DA. Differential distribution of proteins regulating GABA synthesis and reuptake in axon boutons of subpopulations of cortical interneurons. *Cereb Cortex* 21: 2450–2460, 2011. doi:10.1093/cercor/bhr007.

Freund TF, Buzsáki G. Interneurons of the hippocampus. *Hippocampus* 6: 347–470, 1996. doi:10.1002/(SICI)1098-1063(1996)6:4<347:AID-HIPO1>3.0.CO;2-I.

Gerlach AC, Krajewski JL. Antiepileptic drug discovery and development: What have we learned and where are we going? *Pharmaceuticals (Basel)* 3: 2884–2899, 2010. doi:10.3390/ph3092884.

Glausier JR, Fish KN, Lewis DA. Altered parvalbumin basket cell inputs in the dorsolateral prefrontal cortex of schizophrenia subjects. *Mol Psychiatry* 19: 30–36, 2014. [Erratum in *Mol Psychiatry* 19: 140, 2014.] doi:10.1038/mp.2013.152.

Glausier JR, Kimoto S, Fish KN, Lewis DA. Lower glutamic acid decarboxylase 65-kDa isoform messenger RNA and protein levels in the prefrontal cortex in schizoaffective disorder but not schizophrenia. *Biol Psychiatry* 77: 167–176, 2015. doi:10.1016/j.biopsych.2014.05.010.

Hashimoto T, Bazmi HH, Mirnics K, Wu Q, Sampson AR, Lewis DA. Conserved regional patterns of GABA-related transcript expression in the neocortex of subjects with schizophrenia. *Am J Psychiatry* 165: 479–489, 2008. doi:10.1176/appi.ajp.2007.07081223.

Hirsch JC, Agassandian C, Merchán-Pérez A, Ben-Ari Y, DeFelipe J, Esclapez M, Bernard C. Deficit of quantal release of GABA in experi-

mental models of temporal lobe epilepsy. *Nat Neurosci* 2: 499–500, 1999. doi:10.1038/9142.

Hodge RD, Bakken TE, Miller JA, Smith KA, Barkan ER, Graybuck LT, Close JL, Long B, Johansen N, Penn O, Yao Z, Eggermont J, Höllt T, Levi BP, Shehata SI, Aevermann B, Beller A, Bertagnolli D, Brouner K, Casper T, Cobbs C, Dalley R, Dee N, Ding SL, Ellenbogen RG, Fong O, Garren E, Goldy J, Gwinn RP, Hirschstein D, Keene CD, Keshk M, Ko AL, Lathia K, Mahfouz A, Maltzer Z, McGraw M, Nguyen TN, Nyhus J, Ojemann JG, Oldre A, Parry S, Reynolds S, Rimorin C, Shapovalova NV, Somasundaram S, Szafer A, Thomsen ER, Tieu M, Quon G, Scheuermann RH, Yuste R, Sunkin SM, Lelieveldt B, Feng D, Ng L, Bernard A, Hawrylycz M, Phillips JW, Tasic B, Zeng H, Jones AR, Koch C, Lein ES. Conserved cell types with divergent features in human versus mouse cortex. *Nature* 573: 61–68, 2019. doi:10.1038/s41586-019-1506-7.

Isokawa-Akesson M, Wilson CL, Babb TL. Inhibition in synchronously firing human hippocampal neurons. *Epilepsy Res* 3: 236–247, 1989. doi:10.1016/0920-1211(89)90030-2.

Jiang X, Lachance M, Rossignol E. Involvement of cortical fast-spiking parvalbumin-positive basket cells in epilepsy. *Prog Brain Res* 226: 81–126, 2016. doi:10.1016/bs.pbr.2016.04.012.

Klausberger T, Somogyi P. Neuronal diversity and temporal dynamics: the unity of hippocampal circuit operations. *Science* 321: 53–57, 2008. doi:10.1126/science.1149381.

Kleppner SR, Tobin AJ. GABA. In: *Encyclopedia of the Human Brain*. New York: Academic, p. 353–367, 2002.

Kobayashi M, Buckmaster PS. Reduced inhibition of dentate granule cells in a model of temporal lobe epilepsy. *J Neurosci* 23: 2440–2452, 2003. doi:10.1523/JNEUROSCI.23-06-02440.2003.

Lewis DA, Fish KN, Arion D, Gonzalez-Burgos G. Perisomatic inhibition and cortical circuit dysfunction in schizophrenia. *Curr Opin Neurobiol* 21: 866–872, 2011. doi:10.1016/j.conb.2011.05.013.

Löscher W. Critical review of current animal models of seizures and epilepsy used in the discovery and development of new antiepileptic drugs. *Seizure* 20: 359–368, 2011. doi:10.1016/j.seizure.2011.01.003.

Mason GF, Martin DL, Martin SB, Manor D, Sibson NR, Patel A, Rothman DL, Behar KL. Decrease in GABA synthesis rate in rat cortex following GABA-transaminase inhibition correlates with the decrease in GAD(67) protein. *Brain Res* 914: 81–91, 2001. doi:10.1016/S0006-8993(01)02778-0.

Mathern GW, Babb TL, Pretorius JK, Leite JP. Reactive synaptogenesis and neuron densities for neuropeptide Y, somatostatin, and glutamate decarboxylase immunoreactivity in the epileptogenic human fascia dentata. *J Neurosci* 15: 3990–4004, 1995. doi:10.1523/JNEUROSCI.15-05-03990.1995.

Mayerl S, Müller J, Bauer R, Richert S, Kassmann CM, Darras VM, Buder K, Boelen A, Visser TJ, Heuer H. Transporters MCT8 and OATP1C1 maintain murine brain thyroid hormone homeostasis. *J Clin Invest* 124: 1987–1999, 2014. doi:10.1172/JCI70324.

Miles R, Tóth K, Gulyás AI, Hájos N, Freund TF. Differences between somatic and dendritic inhibition in the hippocampus. *Neuron* 16: 815–823, 1996. doi:10.1016/S0896-6273(00)80101-4.

Moyer CE, Delevich KM, Fish KN, Asafu-Adjei JK, Sampson AR, Dorph-Petersen KA, Lewis DA, Sweet RA. Reduced glutamate decarboxylase 65 protein within primary auditory cortex inhibitory boutons in schizophrenia. *Biol Psychiatry* 72: 734–743, 2012. doi:10.1016/j.biopsych.2012.04.010.

Moyer CE, Delevich KM, Fish KN, Asafu-Adjei JK, Sampson AR, Dorph-Petersen KA, Lewis DA, Sweet RA. Intracortical excitatory and thalamocortical boutons are intact in primary auditory cortex in schizophrenia. *Schizophr Res* 149: 127–134, 2013. doi:10.1016/j.schres.2013.06.024.

Mukherji M, Ray AK, Sen PB. Histochemical identification of noradrenaline in fluorescence microscopy by borohydride-periodic acid sequence. *J Histochem Cytochem* 14: 479–482, 1966. doi:10.1177/14.6.479.

O'Sullivan GA, Jedlicka P, Chen HX, Kalbouneh H, Ippolito A, Deller T, Nawrotzki RA, Kuhse J, Kalaidzidis YL, Kirsch J, Schwarzacher SW, Betz H. Forebrain-specific loss of synaptic GABAA receptors results in altered neuronal excitability and synaptic plasticity in mice. *Mol Cell Neurosci* 72: 101–113, 2016. doi:10.1016/j.mcn.2016.01.010.

Pierce JP, Lewin GR. An ultrastructural size principle. *Neuroscience* 58: 441–446, 1994. doi:10.1016/0306-4522(94)90071-X.

Porta EA. Pigments in aging: an overview. *Ann N Y Acad Sci* 959: 57–65, 2002. doi:10.1111/j.1749-6632.2002.tb02083.x.

Prince DA, Jacobs K. Inhibitory function in two models of chronic epileptogenesis. *Epilepsy Res* 32: 83–92, 1998. doi:10.1016/S0920-1211(98)00042-4.

Robinson JM, Takizawa T. Correlative fluorescence and electron microscopy in tissues: immunocytochemistry. *J Microsc* 235: 259–272, 2009. doi:10.1111/j.1365-2818.2009.03221.x.

Rocco BR, DeDionisio AM, Lewis DA, Fish KN. Alterations in a unique class of cortical chandelier cell axon cartridges in schizophrenia. *Biol Psychiatry* 82: 40–48, 2017. doi:10.1016/j.biopsych.2016.09.018.

Rocco BR, Lewis DA, Fish KN. Markedly lower glutamic acid decarboxylase 67 protein levels in a subset of boutons in schizophrenia. *Biol Psychiatry* 79: 1006–1015, 2016a. doi:10.1016/j.biopsych.2015.07.022.

Rocco BR, Sweet RA, Lewis DA, Fish KN. GABA-synthesizing enzymes in calbindin and calretinin neurons in monkey prefrontal cortex. *Cereb Cortex* 26: 2191–2204, 2016b. doi:10.1093/cercor/bhv051.

Schuele SU, Lüders HO. Intractable epilepsy: management and therapeutic alternatives. *Lancet Neurol* 7: 514–524, 2008. doi:10.1016/S1474-4422(08)70108-X.

Sidhu G, Beyene J, Rosenblum ND. Outcome of isolated antenatal hydronephrosis: a systematic review and meta-analysis. *Pediatr Nephrol* 21: 218–224, 2006. doi:10.1007/s00467-005-2100-9.

Simhal AK, Aguerrebere C, Collman F, Vogelstein JT, Micheva KD, Weinberg RJ, Smith SJ, Sapiro G. Probabilistic fluorescence-based synapse detection. *PLOS Comput Biol* 13: e1005493, 2017. doi:10.1371/journal.pcbi.1005493.

Sloviter RS. Decreased hippocampal inhibition and a selective loss of interneurons in experimental epilepsy. *Science* 235: 73–76, 1987. doi:10.1126/science.2879352.

Sloviter RS, Sollas AL, Barbaro NM, Laxer KD. Calcium-binding protein (calbindin-D28K) and parvalbumin immunocytochemistry in the normal and epileptic human hippocampus. *J Comp Neurol* 308: 381–396, 1991. doi:10.1002/cne.903080306.

Somogyi P, Freund TF, Cowey A. The axo-axonic interneuron in the cerebral cortex of the rat, cat and monkey. *Neuroscience* 7: 2577–2607, 1982. doi:10.1016/0306-4522(82)90086-0.

Sweet RA, Fish KN, Lewis DA. Mapping synaptic pathology within cerebral cortical circuits in subjects with schizophrenia. *Front Hum Neurosci* 4: 44, 2010. doi:10.3389/fnhum.2010.00044.

Williamson A, Patrylo PR, Spencer DD. Decrease in inhibition in dentate granule cells from patients with medial temporal lobe epilepsy. *Ann Neurol* 45: 92–99, 1999. doi:10.1002/1531-8249(199901)45:1<92:AID-ART15>3.0.CO;2-N.

Wittner L, Eross L, Czirják S, Halász P, Freund TF, Maglóczky Z. Surviving CA1 pyramidal cells receive intact perisomatic inhibitory input in the human epileptic hippocampus. *Brain* 128: 138–152, 2005. doi:10.1093/brain/awh339.

Wittner L, Eross L, Szabó Z, Tóth S, Czirják S, Halász P, Freund TF, Maglóczky ZS. Synaptic reorganization of calbindin-positive neurons in the human hippocampal CA1 region in temporal lobe epilepsy. *Neuroscience* 115: 961–978, 2002. doi:10.1016/S0306-4522(02)00264-6.

Wittner L, Maglóczky Z, Borhegyi Z, Halász P, Tóth S, Eross L, Szabó Z, Freund TF. Preservation of perisomatic inhibitory input of granule cells in the epileptic human dentate gyrus. *Neuroscience* 108: 587–600, 2001. doi:10.1016/S0306-4522(01)00446-8.

Worrell G, Gotman J. High-frequency oscillations and other electrophysiological biomarkers of epilepsy: clinical studies. *Biomarkers Med* 5: 557–566, 2011. doi:10.2217/bmm.11.74.

Zhang W, Buckmaster PS. Dysfunction of the dentate basket cell circuit in a rat model of temporal lobe epilepsy. *J Neurosci* 29: 7846–7856, 2009. doi:10.1523/JNEUROSCI.6199-08.2009.

Zhang S, Khanna S, Tang FR. Patterns of hippocampal neuronal loss and axon reorganization of the dentate gyrus in the mouse pilocarpine model of temporal lobe epilepsy. *J Neurosci Res* 87: 1135–1149, 2009a. doi:10.1002/jnr.21941.

Zhang W, Yamawaki R, Wen X, Uhl J, Diaz J, Prince DA, Buckmaster PS. Surviving hilar somatostatin interneurons enlarge, sprout axons, and form new synapses with granule cells in a mouse model of temporal lobe epilepsy. *J Neurosci* 29: 14247–14256, 2009b. doi:10.1523/JNEUROSCI.3842-09.2009.

Zhu Y, Stornetta RL, Zhu JJ. Chandelier cells control excessive cortical excitation: characteristics of whisker-evoked synaptic responses of layer 2/3 nonpyramidal and pyramidal neurons. *J Neurosci* 24: 5101–5108, 2004. doi:10.1523/JNEUROSCI.0544-04.2004.